Lawrence Berkeley National Laboratory
Recent Work

Title
ACCURATE MEASUREMENT OF NOISE PARAMETERS IN ULTRA-LOW NOISE OPTO-FEEDBACK SPECTROMETER SYSTEMS

Permalink
https://escholarship.org/uc/item/0549m4w9

Author
Llacer, Jorge.

Publication Date
1975-05-01

eScholarship.org Powered by the California Digital Library
University of California

U U ... 4 3 0 1 4 5 5

Presented at the 2nd ISPRA Nuclear Electronics Symposium, Stresa, Italy, May 20 - 23, 1975

LBL-3671
c.1

RECEIVED
LAWRENCE
BERKELEY LABORATORY

JUL 17 1975

LIBRARY AND
DOCUMENTS SECTION

ACCURATE MEASUREMENT OF NOISE PARAMETERS IN ULTRA-LOW NOISE OPTO-FEEDBACK SPECTROMETER SYSTEMS

Jorge Llacer

May 1975

Prepared for the U. S. Energy Research and Development Administration under Contract W-7405-ENG-48

For Reference

Not to be taken from this room

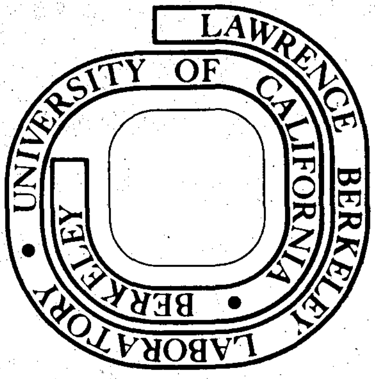

LBL-3671
c.1

DISCLAIMER

This document was prepared as an account of work sponsored by the United States Government. While this document is believed to contain correct information, neither the United States Government nor any agency thereof, nor the Regents of the University of California, nor any of their employees, makes any warranty, express or implied, or assumes any legal responsibility for the accuracy, completeness, or usefulness of any information, apparatus, product, or process disclosed, or represents that its use would not infringe privately owned rights. Reference herein to any specific commercial product, process, or service by its trade name, trademark, manufacturer, or otherwise, does not necessarily constitute or imply its endorsement, recommendation, or favoring by the United States Government or any agency thereof, or the Regents of the University of California. The views and opinions of authors expressed herein do not necessarily state or reflect those of the United States Government or any agency thereof or the Regents of the University of California.

0

0 0 0 0 4 3 0 1 4 5 6

4 3 0 1 4 3 6

ACCURATE MEASUREMENT OF NOISE PARAMETERS IN ULTRA-LOW NOISE OPTO-FEEDBACK SPECTROMETER SYSTEMS*

Jorge Llacer

Lawrence Berkeley Laboratory
University of California
Berkeley, California 94720 U.S.A.

ABSTRACT

The accurate measurement of the basic noise parameters of ultra-low noise spectrometer systems has been developed in the frequency domain by spectrum analysis. This method overcomes some of the difficulties experienced in using conventional techniques. An analytic and experimental comparison between 'time' and frequency domain techniques is carried out and the use of the latter as a method to develop extremely low-noise detector and FET packages is demonstrated. The origin of the remaining noise in high quality systems is traced to surface and gate junction generation through traps in the FET.

CONTENTS

I. INTRODUCTION 1
II. GENERAL TREATMENT OF FILTERING IN TIME DOMAIN 2
A. Main Formulation 2
B. Treatment Of Individual Noise Sources . 3
1. Detector and FET leakage currents . . . 3
2. Parallel resistance noise 3
3. Series noise resistances 3
4. f^{α}-type noises 4
C. Evaluation Of Noise Constants $<N^2>$ . . . 5
III. QUANTITATIVE NOISE ANALYSIS IN FREQUENCY DOMAIN 6
A. Main Formulation 6
B. Treatment Of Individual Noise Sources . 7
1. Detector and FET leakage currents . . . 7
2. Parallel resistance noise 7
3. Series noise resistances 7
4. 1/f noise series sources 7
5. f-noise parallel source 7
C. Evaluation Of Noise Parameters 8
IV. RESULTS OF MEASUREMENTS 8
A. Comparative Measurements 8
B. Germanium System Design Experiments . . . 10
1. Detector fabrication and characteristics 10
2. Effect of detector mount on noise . . . 11
3. Effect of Boron Nitride FET mount . . . 12
4. Effect of feedback capacitor dielectric 13
5. Searching for the origin of 1/f noise. . 14
V. CONCLUSIONS 16
VI. ACKNOWLEDGEMENTS 16
REFERENCES 16

I. INTRODUCTION

The approximate measurement of the dominant parameters determining the electronic noise performance of nuclear spectrometer systems with solid state detectors is a well known technique. It is based on the dependence of electronic resolution on main amplifier peaking time and it has been treated extensively in the literature, as for example in Ref. 1, for simple RC-CR filters. For more complex filtering, the shape of the step response of the main amplifier determines a set of factors which are needed in order to estimate system noise parameters. Goulding has calculated a set of such factors for the series and parallel noise sources in a variety of filtering conditions[2].

For a more accurate characterization of the noise sources in spectrometer systems, Radeka has developed a technique which allows the measurement of noise parameters with a higher degree of sophistication[3]. Such techniques are based on separating the series and parallel noise contributions by scaling down to low input capacitance the results of a measurement of noise vs time constant carried out with an added high capacitance.

Although the usefulness of the above methods is certain for noise analysis of most spectrometer systems, they present some problems in attempting to characterize accurately the noise sources of ultra-low noise opto-feedback systems (below 90 eV FWHM at peaking times above 60 μs, for example). The main limitations observed are the following:

* This work was performed under the auspices of the United States Energy Research and Development Administration.

1) Presently available main amplifiers and pulsers do not provide the capability for obtaining sufficient data points at long time constants to separate the parallel and 1/f type noises.

2) The presence of small amounts of hum and microphonics can mask the more basic noise characteristics of a system and inconsistent values for parallel, and 1/f noise parameters are obtained under slightly different measurement conditions (changing cable lengths and configuration, for example).

3) Plots of resolution vs peaking time at short values of the latter do not appear generally as straight lines with a slope of -1/2 when plotted on logarithmic paper, making the determination of the series contribution to noise uncertain. This is due to rise time limitations of the preamplifier affecting the overall step response of the filter.

4) The addition of a high input capacitance for the separation of the individual components of noise, using the technique developed by Radeka[3] results in the introduction of a high dielectric loss f-type noise and of disturbances in the mechanical and thermal environments of the FET preventing accurate determination of noise parameters in ultra-low noise systems.

Fortunately, the above difficulties can be overcome in a useful manner by making measurements in frequency domain. With a spectrum analyzer of narrow bandwidth (5-20 Hz, for example), a set of measurements at spot frequencies between 100 Hz and 20 KHz yields results of RMS noise vs frequency, which can be analyzed readily with the help of a small desk computer. The final result is a set of parameters which are obtained with sufficient accuracy to permit comparisons and optimization by small changes in the design or operating conditions of a system.

The basic difference between the 'time' and frequency domain measurements is that the 'time domain' methods use integrals over wide bandwidths while frequency domain uses integrals over very narrow bandwidths. For detailed work the latter provides much more precise information about the characteristics of a noise spectrum.

The purpose of this paper will then be to present an analytic and experimental comparison between 'time' and frequency domain techniques and to illustrate the use of the latter as a tool to develop extremely low noise detector and FET packages.

First, filtering in the 'time domain' will be treated in some detail for the purpose of providing checkpoints for the frequency domain measurements, next the quantitative theory of a spectrum analyzer will be described. Finally, comparative measurements and system design experiences will be reported.

II. GENERAL TREATMENT OF FILTERING IN TIME DOMAIN

A. Main Formulation

The filtering of series and parallel noise sources in nuclear spectrometry amplifiers has been studied quite extensively in time domain with the advantage over frequency domain analysis that the behavior of even non-linear, time variant filters can be predicted[2,4,5]. In this section a quantitative general treatment for noise sources with arbitrary power spectral density $S_n(f)$ will be developed, restricted, however, to linear time invariant filtering. The treatment is only different from the ones referenced above in that it is kept completely quantitative.

Consider a generalized noise source with power spectral density $S_n(f)$ which is filtered in two steps, by a charge sensitive amplifier and a main filtering amplifier. Let $h_1(t)$ be the response function of the charge sensitive loop for a δ-function source of the same nature (voltage or current) as the noise source considered. The δ-function source is located at the same place in the circuit as the noise source. The voltage impulse response function of the main amplifier will be defined as $h_2(t)$. The complete impulse response function is, then, $g(t) = h_1(t) * h_2(t)$, where $*$ denotes convolution. The complete transfer function is $G(f) = H_1(f)\, H_2(f)$ and the power spectral density of the output will be

$$S_k(f) = S_n(f)\,|G(f)|^2 \qquad (1)$$

The autocorrelation function $R_k(\tau)$ at the output of the filter is the Fourier transform of $S_k(f)$ and its value at $\tau = 0$,

$$R_k(0) = \int_{-\infty}^{\infty} S_k(f)\,df = W_k \qquad (2)$$

is the total noise power at the output due to the particular source k under consideration.

Transforming Eq. (1) we obtain

$$W_k = \int_{-\infty}^{\infty} d\tau\; R_n(\tau) \int_{-\infty}^{\infty} dt\; g(t)\; g(t+\tau) \qquad (3)$$

where $R_n(\tau)$ is the autocorrelation of the noise source. This is a general result which will be applied to specific noise sources below.

Presentation of measured noise in terms of Noise Line Width (NLW) requires the normalization of the result of Eq. (3) to the maximum of the response of the system to a unit charge impulse at the input. Letting $g_Q(\tau_o)$ be the value of such a maximum, one can express the contribution to noise line width from several noise sources by

$$\mathrm{NLW(FWHM)} = \frac{2.35\,\bar{\varepsilon}}{q}\left(\frac{\Sigma_k W_k}{\{g_Q(\tau_o)\}^2}\right)^{1/2} \tag{4}$$

where the W_k's have to be computed from Eq. (3) by choosing the proper R_n and g functions, $\bar{\varepsilon}$ is the energy needed to create one electron-hole pair in the detector and q is the electronic charge.

B. Treatment Of Individual Noise Sources

Figure 1 shows the general model for the noise sources and preamplifier circuit to be discussed here. In the treatment which follows the feedback network is considered a part of the transfer function $h_1(t)$. This results in the separation of contributions from series sources into sources inside and sources outside the feedback loop, which behave differently.

1. Detector and FET leakage currents:

For the expected case of $r_p \gg r_{sd}$ and for frequencies such that $1/\omega C_d \gg r_{sd}$ the two sources i_L and i_g are effectively in parallel. The transfer function $H_1(f)$ of the preamplifier is given approximately by

$$H_1(f) = \frac{V_{out}\,(f)}{i_L\,(f)} = \frac{A(f)}{j\omega(C_d+C_g) + Y_{fb}(1-A(f))} \tag{5}$$

where $Y_{fb} = 1/R_{fb} + j\omega C_{fb}$. For frequencies such that $|A(f)|$ is large, the transfer function is determined mostly by the feedback network. In a simplified form, with $|A(f)| \gg 1$, Eq. (5) becomes

$$H_1(f) = \frac{1}{G_{fb} + j\omega C_{fb}} \tag{6}$$

The corresponding impulse response $h_1(t)$ is then

$$h_1(t) = \frac{1}{C_{fb}}\exp(-t/\tau_{fb}),\ t > 0 \tag{7}$$

where $\tau_{fb} = R_{fb}\,C_{fb}$.

For R_{fb} very large, $g(t) = h_1(t) * h_2(t)$ is basically the step response of the main amplifier.

The power spectral density of these sources, for pure shot noise, is given by $q(I_L + I_g)$, for $-\infty<f<\infty$, (white noise) and its autocorrelation is $R_n(\tau) = q(I_L + I_g)\,\delta(\tau)$. Substituting in Eq. (3) and integrating we find

$$W_k = q(I_L + I_g)\int_{-\infty}^{\infty}\{g(t)\}^2\,dt \tag{8}$$

One can obtain g(t) accurately from a preamplifier-amplifier combination by injecting a fast charge pulse to the preamplifier input and obtaining the waveform at the filter amplifier output. This measurement includes, then, the frequency response of the preamplifier and main amplifier. Defining

$$\frac{\int_{-\infty}^{\infty}\{g(t)\}^2\,dt}{\{g_Q(\tau_o)\}^2} \triangleq \langle N_s^2\rangle \tag{9}$$

in agreement with Goulding's notation[2], the normalized noise power contribution from the parallel current sources is

$$\frac{W_k}{\{g_Q(\tau_o)\}^2} = qI_L'\,\langle N_s^2\rangle \tag{10}$$

where $I_L' = I_L + I_g$.

2. Parallel resistance noise:

The two voltage noise generators v_p and v_{fb} can be converted to equivalent current sources with behavior identical to the current sources of the previous section.

If we let r_p' be the parallel combination of r_p and r_{fb}, we can use the above development with a noise power spectral density given by $2kT/r_p'$, so that the noise power contribution from this source becomes

$$\frac{W_k}{\{g_Q(\tau_o)\}^2} = \frac{2kT}{r_p'}\,\langle N_s^2\rangle \tag{11}$$

3. Series noise resistances:

The transfer functions for the voltage noise sources v_{sd} (caused by detector series resistance) and v_s (FET channel resistance transferred to the gate) are not identical since the generators are outside and inside the feedback loop, respectively.

For the case of the detector series resistance, with r_p' very large and A(f) large and constant, the transfer function is given by

$$\frac{V_{out}}{v_{sd}} \simeq \frac{C_d}{C_{fb}} \tag{12}$$

while for the FET noise the transfer function is

$$\frac{V_{out}}{v_s} \simeq 1 + \frac{C_g + C_d}{C_{fb}} = \frac{C_{in}}{C_{fb}} \qquad (13)$$

where C_{in} is the total input capacitance.

The power spectral densities of the sources are given by 2kT r_{sd} and 2kT r_s. It is possible to simplify the notation by defining a single series resistance r_s' to be placed inside the feedback loop with a value

$$r_s' = r_s + \frac{r_{sd}\, C_d^2}{C_{in}^2} \qquad (14)$$

Then, the transfer function is approximately a constant, given by Eq. (13) and the power spectral density is 2kT r_s'. This implies that a series resistance external to the feedback circuit is less noisy than one inside the feedback loop. The autocorrelation function for these noise sources is, then

$$R_n(\tau) = 2kT\, r_s'\, \delta(0) \qquad (15)$$

In order to find the equivalent noise contribution, we use Eq. (3) realizing that $g(t) = h_1(t) * h_2(t) \simeq (C_{in}/C_{fb})\, h_2(t)$, since $h_1(t)$ is approximately a δ-function. Then

$$W_k = 2kT\, r_s' \left(\frac{C_{in}}{C_{fb}}\right)^2 \int_{-\infty}^{\infty} \left\{h_2(t)\right\}^2 dt \qquad (16)$$

Normalizing and defining

$$\frac{\left(1/C_{fb}^2\right) \int_{-\infty}^{\infty} \left\{h_2(t)\right\}^2 dt}{\left\{g_Q(\tau_o)\right\}^2} \triangleq \langle N_\Delta^2 \rangle \qquad (17)$$

we obtain the power noise contribution from series sources to be

$$\frac{W_k}{\left\{g_Q(\tau_o)\right\}^2} = 2kT\, r_s'\, C_{in}^2 \langle N_\Delta^2 \rangle \qquad (18)$$

In practice, the impulse response function $h_2(t)$ of Eq. (17) can be obtained by differentiating numerically the waveform at the output of the filter when the preamplifier is excited by very short input current pulses. It can be shown that the obtained $h_2(t)$ is indistinguishable for all purposes from what would be obtained by injecting δ-functions of voltage at v_s or v_{sd}.

4. f^α-type noises:

Here we are going to be concerned with noise sources with power spectral densities of the form $(A/2)|f|^\alpha$ where α can have any value, in principle. For $\alpha = -1$ we have the well known 1/f noise in detectors and FETs, and for $\alpha = 1$ we have lossy insulator noise.

The evaluation of Eq. (3) for an arbitrary value of α presents serious difficulties in the time domain because of the need to have $R(\tau)$, the Fourier transform of $|f|^\alpha$ which is, in general, not obtainable. It is, however, possible to work in the frequency domain by evaluating approximately Eq. (2) using Eq. (1). By defining suitable frequency cutoffs for the integrals the errors incurred are kept quite small. We can then write

$$W_k = \frac{A}{2} \int_{-\infty}^{\infty} |f|^\alpha \left| F\left\{g(t)\right\} \right|^2 df \qquad (19)$$

with g(t) being the waveform at the output of the main amplifier for an impulse at the source location considered.

We consider first series 1/f noises, as voltage generators at locations v_s and v_{sd} of Fig. 1. We can define a parameter A' to cover both sources in analogy to Eq. (14) as

$$A' = A_s + \frac{A_{sd}\, C_d^2}{C_{in}^2} \qquad (20)$$

The power spectral density of this combined noise source is then $(A'/2)|f|^{-1}$ and the appropriate impulse response function to go into Eq. (19) is the derivative of the filter output waveform, or $h_2(t)$. Since $F\{h_2(t)\} = i\omega\, F\{g(t)\}$, where g(t) is the step response function of the filter, we can define

$$\langle N_{-1s}^2 \rangle \triangleq \frac{\left(1/C_{fb}^2\right) \int_{-\infty}^{\infty} |f|^{-1} \left| i\omega\, F\left\{g(t)\right\} \right|^2 df}{\left\{g(\tau_o)\right\}^2} \qquad (21)$$

and the noise power contribution from series 1/f sources is

$$\frac{W_k}{\left\{g_Q(\tau_o)\right\}^2} = \frac{A'}{2}\, C_{in}^2 \langle N_{-1s}^2 \rangle \qquad (22)$$

Next we consider a 'parallel lossy dielectric', as described by Radeka[3]. For a dielectric with loss factor D, considered to be a constant, placed in parallel with the input, the transfer function will be identical to the case of parallel resistance noise, with g(t) in Eq. (19) being the actual filter output waveform and the source converted to its equivalent Norton current source.

The power spectral density of this voltage noise source will be given by $2kT\ R(\omega)$, with the corresponding current source of the form $2kT\ G(\omega) = 2kT\ (DC_{d1})|\omega|$, where $D = G/|\omega|C_{d1}$ and C_{d1} is the dielectric capacitance. For this noise source, if we define

$$\frac{\int_{-\infty}^{\infty} 2\pi\ |\omega|\ \left|F(g(t))\right|^2 df}{\left\{g(\tau_o)\right\}^2} \triangleq \langle N_{+1p}^2\rangle \tag{23}$$

we observe that $\langle N_{+1p}^2\rangle \equiv \langle N_{-1s}^2\rangle$ of Eq. (23). The power noise contribution from this source is, therefore, expressing DC_{d1} as $G_o/2\pi f_o$, following Radeka, given by

$$\frac{W_k}{\left\{g_Q(\tau_o)\right\}^2} = \frac{kT\ G_o}{2\pi^2 f_o} \langle N_{+1p}^2\rangle \tag{24}$$

where G_o is the conductance measured at frequency f_o.

C. Evaluation of Noise Constants $\langle N^2\rangle$

For the purpose of obtaining information on absolute magnitudes of equivalent noise resistances, currents, etc. it is necessary to evaluate $\langle N_S^2\rangle$, $\langle N_\Delta^2\rangle$, and $\langle N_{-1s}^2\rangle$ from Eqs. (9), (17) and (21).

Calculations have been carried out for a filter with step response function of form $g(t) = (t/\tau_o)^n \exp[n(1-t/\tau_o)]$ which approaches a Gaussian as n becomes large. These calculations have been carried out from n = 1 (RC-CR filter) to n = 7. Next, the actual output waveforms of three different main amplifiers of current use at the Lawrence Berkeley Laboratory have been studied by sampling their step responses at 512 points and carrying out a numerical integration procedure for evaluation of the corresponding expressions. Difficulties with the differentiation of the experimental results have been minimized by differentiating a least squares fitted curve over four points at every point. Even then, some uncertainties have resulted in the calculations of $\langle N_\Delta^2\rangle$ because of noise in the sampling oscilloscope/ADC system.

Table 1 gives the results for the theoretical 'pseudo-gaussian' filter, with τ_o being the peaking time.

The calculated value of $\langle N_{-1s}^2\rangle$ for n = 1 is close to the theoretical value of $e^2 = 7.39$ (Ref. 3 for example), and, as n becomes larger, $\langle N_{-1s}^2\rangle$ is seen to approach the value of 2π, which is the theoretical result for a pure Gaussian filter.

TABLE 1

Order n	$\langle N_S^2\rangle$	$\langle N_\Delta^2\rangle$	$\langle N_{-1s}^2\rangle$
1	$1.85/\tau_o$	$1.85/\tau_o$	7.54
2	1.28	1.71	6.90
3	1.04	1.87	6.67
4	.90	2.05	6.56
5	.80	2.22	6.50
6	.73	2.38	6.46
7	.67	2.54	6.43

Table 2 gives the corresponding results for three real amplifiers, indicating the true peaking time (1% to 100%) as a function of setting of the time constant switch. Effects due to preamplifier and main amplifier rise times are apparent. A pulser with a rise time better than 10 ns was used at the short time constants. The amplifiers used are LBL Model 101 (one double pole active integrator), LBL Model 550 (one double pole active, one single passive) and LBL Model 848 (three double active, one single passive). The preamplifier is a standard pulsed opto X-ray system with a Si(Li) detector.

TABLE 2

Amplifier Model	Setting	τ_o	$\langle N_S^2\rangle/\tau_o$	$\langle N_\Delta^2\rangle \times \tau_o$	$\langle N_{-1s}^2\rangle$
LBL 101	.2 μs	.34 μs	.95	1.87	6.67
	.4	.512	1.00	1.87	6.78
	.8	.85	1.12	1.72	6.75
	1.6	1.56	1.15	(1.70)	6.86
	3.2	2.64	1.28	1.66	6.93
	6.4	5.50	1.24	1.67	6.81
LBL 550	.25	.396	.82	2.13	6.57
	.50	.67	.86	2.06	6.50
	1.0	1.29	.90	2.02	6.90
	2.0	2.44	1.02	(1.95)	7.28 ?
	4.0	4.36	1.05	(1.90)	7.00
	8.0	7.70	1.07	(1.87)	6.56
LBL 848		6.90	.79	2.46	6.66
		28.20	.75	2.54	6.86

Note: Figures in parenthesis indicate estimates by interpolation and/or comparison with values from Table 1.

The slow but gradual improvement of $\langle N_{-1s}^2 \rangle$ as the order of the 'pseudo-gaussian' increases, (see Table 1) is not clearly obtained in the calculations based on actual amplifier waveforms. It is believed that noise in the waveform sampling procedure transforms itself in some random high frequency component that causes errors in the evaluation of $\langle N_{-1s}^2 \rangle$. One can estimate an experimental value of $\langle N_{-1s}^2 \rangle \simeq 6.85 \pm .1$ for all the amplifier considered with a very tolerable expected error.

It is now convenient to summarize the results of the time domain analysis by adding the contributions of the noise sources treated. It is then found, from Eqs. (4), (10), (11), (18), (22) and (24) that

$$\mathrm{NLW(FWHM)} = \frac{2.35\,\bar{\varepsilon}}{q}\left\{\left(q\,I_L' + \frac{2kT}{r_p'}\right)\langle N_s^2\rangle + 2kT\,r_s'\,C_{in}^2\,\langle N_\Delta^2\rangle + \left(\frac{A'}{2}\,C_{in}^2 + \frac{A_f}{2}\right)\langle N_{-1s}^2\rangle\right\}^{1/2} \quad (25)$$

where

$$I_L' = I_L + I_g,$$

$$\frac{1}{r_p'} = \frac{1}{r_p} + \frac{1}{r_{fb}},$$

$$r_s' = r_s + r_{sd}\left(\frac{C_d}{C_{in}}\right)^2,$$

$$A' = A_s + A_{sd}\left(\frac{C_d}{C_{in}}\right)^2 \quad \text{and}$$

$$A_f = \frac{kT\,G_o}{\pi^2\,f_o}.$$

III. QUANTITATIVE NOISE ANALYSIS IN FREQUENCY DOMAIN

A. Main Formulation

The mathematical formulation of a spectrum analyzer can be given as follows: consider a noise source with power spectrum $S_n(f)$, $-\infty<f<\infty$, which is being analyzed with an instrument whose bandpass is characterized by a function $H_b(f) = H_o[I(f-f_o) + I(f+f_o)]$, where $I(f)$ is symmetrical about zero frequency, $I(0) = 1$, and f_o is the frequency being analyzed. The power spectrum at the output of the analyzer bandpass filter is then:

$$S_{out}(f) = S_n(f)\,|H_b(f)|^2 = H_o^2\,S_n(f)\,|I(f-f_o) + I(f+f_o)|^2 \quad (26)$$

If the bandpass filter is followed by a square law detector and the input noise is Gaussian, it can be shown that the power spectral density of the output of the detector, $S_{out^2}(f)$, is given by

$$S_{out^2}(f) = R_{out}^2(0)\,\delta(f) + 2\,(S_{out}(f) * S_{out}(f)) \quad (27)$$

If we look only at the RMS dc part of the detected signal, $R_{out}(0)$ with other frequency components suitably filtered out, we have

$$R_{out}(0) = \int_{-\infty}^{\infty} S_{out}(f)\,df = \int_{-\infty}^{\infty} H_o^2\,S_n(f)\,|I(f-f_o) + I(f+f_o)|^2\,df \simeq 2\,H_o^2\,S_n(f_o)\int_{-\infty}^{\infty} I^2(f)\,df \quad (28)$$

for narrow bandwidth filters and f_o such that there is no overlap between $I(f-f_o)$ and $I(f+f_o)$. Defining

$$\Delta f \triangleq \int_{-\infty}^{\infty} I^2(f)\,df \quad (29)$$

as the power bandwidth of the analyzer for noise, we see that the expected value of the output of a square law detector is a quantity

$$W(f_o) = 2\,H_o^2\,\Delta f\,S_n(f_o) \quad (30)$$

i.e., $W(f_o)$ is proportional to the power spectral density of the input noise.

A simple form of spectrum analyzer does not use a square law detector, but instead uses a half wave (more or less) ideal rectifier with suitable filtering to obtain the magnitude of the envelope of the i.f. signal formed by heterodyning the noise with a local oscillator. Fortunately, for narrow band Gaussian processes (i.e., a Gaussian process passed through a narrow filter), there is a simple relationship between the expected value of the envelope (as measured by the half wave 'linear' rectifier) and the square root of the expected value of the envelope squared (as seen by a square law detector)[6]. This relationship, with $Z(t)$ representing the envelope, can be expressed as

$$\frac{E(Z)}{[E(Z^2)]^{1/2}} = \frac{\pi^{1/2}}{2} = .886 \quad (31)$$

Since $E(Z^2)$ corresponds to $W(f_o)$ of Eq. (30), we see that one can measure the RMS spectrum of the noise source by using the 'linear' analyzer. Combining Eqs. (30) and (31) we have

$$[S_n(f_o)]^{1/2} = \frac{E(Z)}{.886 \times \sqrt{2}\, H_o\, \Delta f^{1/2}} \qquad (32)$$

We are left only with the need to evaluate the normalization constant H_o. The particular instrument used for the present work is calibrated in such a way that the peak of $H_o I(f)$ corresponds to the RMS value of a pure sinusoidal wave at the input. For an input A cos $\omega_o t$ at frequency f_o, the voltage spectrum at the output of the bandpass filter is

$$G_{out}(f) = H_o \frac{A}{2} [I(f-f_o) + I(f+f_o)]\, [\delta(f-f_o) + \delta(f+f_o)] \qquad (33)$$

with a power spectrum given by

$$S_{out}(f) = |G(f)|^2 \qquad (34)$$

If looked at by a square law detector, the RMS dc part of the detected signal is, by analogy with Eq. (28),

$$R_{out}(0) = \int_{-\infty}^{\infty} |G(f)|^2\, df = H_o^2 \frac{A^2}{4} \cdot 2\, [I(0)]^2 = H_o^2 \frac{A^2}{2} \qquad (35)$$

Since the expected value of the envelope of a steady amplitude sinewave seen by a 'linear' detector is simply the square root of the expected value for a square law detector, E(Z) has the value

$$E(Z) = H_o A/\sqrt{2} \qquad (36)$$

In order for this value to correspond to the RMS value of the input cosine wave, which is what the analyzer measures, we have to set $H_o = 1$. We have, finally, from Eq. (32)

$$[S_n(f_o)]^{1/2} = \frac{E(Z)}{.886 \times \sqrt{2}\, \Delta f^{1/2}} \qquad (37)$$

with E(Z) being the reading of the spectrum analyzer, and Δf given by Eq. (29).

B. Treatment Of Individual Noise Sources

The power spectra of the principal noise sources at their origin and after the pre-filtering by the capacitively fedback preamplifier have already been obtained in part II section B of this report and it will be only necessary to summarize them here, with the simplifying assumptions discussed in that section. S_1 corresponds to noise power density at the source, S_2 is at the output of the preamplifier.

1. Detector and FET leakage currents:

$$S_1(f) = q(I_L + I_g) = q\, I_L'$$

$$S_2(f) = q\, I_L' \left|\frac{1}{G_{fb} + j\omega C_{fb}}\right|^2 = q\, I_L' \cdot \frac{1}{G_{fb}^2 + \omega^2 C_{fb}^2} \qquad (38)$$

For opto-feedback systems with

$$G_{fb} \simeq 0,\; S_2(f) \simeq q\, I_L'/\omega^2 C_{fb}^2 \qquad (39)$$

2. Parallel resistance noise:

$$S_1(f) = 2kT/r_p'$$

$$S_2(f) = \frac{2kT}{r_p'} \cdot \frac{1}{G_{fb}^2 + \omega^2 C_{fb}^2} \qquad (40)$$

3. Series noise resistances:

$$S_1(f) = 2kT\, r_s' \text{ , where } r_s' = r_s + \frac{r_{sd}\, C_d^2}{C_{in}^2}$$

$$S_2(f) = 2kT\, r_s' \left(\frac{C_{in}}{C_{fb}}\right)^2 \qquad (41)$$

4. 1/f noise series sources:

$$S_1(f) = \frac{A'}{2} \frac{1}{f} \text{ , where } A' = A_s + \frac{A_{sd}\, C_d^2}{C_{in}^2}$$

$$S_2(f) = \frac{A'}{2} \frac{1}{f} \left(\frac{C_{in}}{C_{fb}}\right)^2 \qquad (42)$$

5. f-noise parallel source:

$$S_1(f) = \frac{2kT\, G_o}{f_o}\, f$$

$$S_2(f) = \frac{2kT\, G_o}{f_o} \frac{f}{G_{fb}^2 + \omega^2 C_{fb}^2} \quad (43)$$

For $G_{fb} \simeq 0$, $$S_2(f) = \frac{2kT\, G_o}{(2\pi)^2 f_o} \frac{1}{f} \frac{1}{C_{fb}^2} \quad (44)$$

Since sources 4. and 5. have identical frequency dependence and cannot immediately be separated from each other, they can be lumped into one single expression:

$$S_2(f) = A_\alpha \frac{1}{f} \frac{1}{C_{fb}^2} \quad (45)$$

where $$A_\alpha = \frac{A'}{2} C_{in}^2 + \frac{A_f}{2} \quad (46)$$

C. Evaluation of Noise Parameters

The objective of the measurements in frequency domain is to obtain $S_2(f)$, the noise spectrum at the output of the preamplifier and from $S_2(f)$ find values for the parameters I_L', $r_s' C_{in}^2$ and A_α for opto-feedback amplifiers, assuming $G_{fb} \simeq 0$. These parameters are defined in Eqs. (25) and (46). For this purpose, the preamplifier output is connected to a low-noise wide-band amplifier with gain G at all the frequencies of interest, and the amplified noise is spectrum analyzed.

For the measurements described in this paper an ancient vacuum tube Panoramic Model LP-1a spectrum analyzer has been used. It operates approximately between 10 Hz and 20 KHz with variable bandwidths down to approximately 2 Hz, and an intermediate frequency of 100 KHz. For accurate measurements of $S_2(f)$ it is necessary to use a sharp low-pass filter with cut-off at 50 to 60 KHz in order to remove preamplifier noise at 100 KHz (the i.f. of the analyzer) which would otherwise interfere with the measurements. Also, the analyzer detector has been modified by gating its integrator so that it does not charge or discharge during the transients due to the opto reset.

The effective noise bandwidth Δf of the analyzer at a switch position BW = 25 has been obtained from Eq. (29) by measuring, squaring and integrating the sweep waveform obtained from a pure sinewave. At positions below BW = 25, the values of Δf have then been obtained by comparing white noise measurements. The results are given in Table 3. A LBL Model 101 main amplifier in a wideband configuration has been used for the measurements, with a gain G = 1970 ± 35 at maximum settings and a flat response above 50 cps.

TABLE 3

BW SETTING	$\Delta f^{1/2}$
25	5.23
10	3.30
5	2.31

The RMS noise readings obtained at a finite set of frequencies are then analyzed by fitting a function of the form

$$Z(f) = \left[\frac{a_1}{f^2} + \frac{a_2}{f} + a_3\right]^{1/2} \quad (47)$$

so as to minimize χ^2 error, with weights equal to the reciprocal of the values at the experimental points. Eq. (39), (41), (45) and (46) provide the relationships

$$I_L' = \frac{a_1\, C_{fb}^2\, (2\pi)^2}{2\, q} \quad (48)$$

$$A_\alpha = \frac{a_2\, C_{fb}^2}{2} \quad (49)$$

$$r_s'\, C_{in}^2 = \frac{a_3\, C_{fb}^2}{4kT} \quad (50)$$

with the function Z(t) given by the analyzer readings divided by 0.886 $\Delta f^{1/2}$, from Eq. (37). The measurement of C_{fb} is straight forward and can be obtained within a few percent error.

An alternative method of fitting Eq. (47) to measurement data has been to plot the experimental points on the CRT of a desk computer and vary the parameters of Eq. (48) to (50), interacting with the computer, to obtain a visual best fit. This method has been found to be more satisfactory than a straight mathematical fit because one can judge easily if there are any points which must be discarded due to measurement inaccuracies or errors.

IV. RESULTS OF MEASUREMENTS

A. Comparative Measurements

The purpose of the measurements reported in this section is to establish the correspondence between the measurements in 'time' and frequency domains and to point out the strengths and weaknesses of both methods in the noise analysis of very high-resolution systems. Measurements have been made of a moderately good Si(Li) opto-feedback detector system with an optimum electronic resolution of approximately 90 eV FWHM at a peaking time τ_o = 65 μs.

Noise line widths as a function of time constant setting have been obtained by standard methods. Two different main amplifiers have been used to check on consistency of the results at short time constants. The results are shown in Table 4 and plotted in Fig. 2 as a function of the true measured peaking time τ_o. The noise behavior over the range of peaking time less than approximately $\tau_o \approx 4$ μs is dominated by the series equivalent noise resistances. In that region, Eq. (25) yields

$$r_s^{'1/2} C_{in} = \frac{NLW}{(2.35\bar{\varepsilon}/q)\ (2kT\ \langle N_\Delta^2\rangle)^{1/2}}$$

$$= \frac{NLW(FWHM)\,eV}{2.929 \times 10^9\ \langle N_\Delta^2\rangle^{1/2}} \qquad (51)$$

for silicon at 77°K, equivalent noise resistance at 100°K.

TABLE 4

Amplifier Model	τ_o(true)	NLW(FWHM) (eV)	$(\langle N_\Delta^2\rangle)^{1/2}$	$r_s^{'1/2} C_{in}$
LBL 101	.3 μs	735	2479	1.01×10^{-10}
	.51	595	1910	1.06×10^{-10}
	.85	430	1421	1.03×10^{-10}
	1.56	306	1101	1.17×10^{-10}
	2.64	224	791	9.65×10^{-11}
LBL 550	.4	672	2310	9.93×10^{-11}
	.67	525	1750	1.02×10^{-10}
	1.29	357	1250	9.75×10^{-11}
	2.50	248	893	9.50×10^{-11}
	4.36	189	660	9.77×10^{-11}
	8.40	141	492	-
	17.0	108	331	-
	34	94	-	-
	65	90	-	-
	140	91	-	-

Using the values of $\langle N_\Delta^2\rangle$ shown in Table 2 for the two amplifiers studied, a value of $r_s^{'1/2}$ C_{in} has been calculated at each relevant point and the results are also shown in Table 4. From the nine measurements one obtains a value of $r_s^{'1/2} C_{in} = 1.01 \times 10^{-10}$ with a standard deviation of 0.05×10^{-10}. If one assumes $C_{in} = 5$ pf, r_s' becomes 408 Ω, and for a measured detector capacitance of 1.25 pF, one obtains from Eq. (18) the relation $r_s' = 408\ \Omega = r_s + 0.057\ r_{sd}$ giving an indication of how the equivalent series resistance may be divided between the FET and the detector.

The parallel and f^α noise components of the system cannot be evaluated with any accuracy with the data points available at long τ_o.

Using the techniques described in Sec. III C frequency domain measurements were carried out at 14 points between 150 Hz and 20 KHz. The results of RMS noise at the output of the preamplifier, corrected to $\Delta f = 1$ Hz, are shown in Fig. 3. The values plotted correspond to $\sqrt{2}\,[S_n(f)]^{1/2}$.

Using all 14 measurement points, the nonlinear minimum χ^2 fitting procedure results in the values for the noise parameters shown in Table 5. The corresponding fitting function values are also shown in Fig. 3.

The results of using only the five measurement points indicated by arrows in Fig. 3 for the fitting procedure are also shown in Table 5. The obtained parameter values are within less than 10% from the 14-point values, but should be considered less correct, as measurement errors do not average out so well with fewer points.

TABLE 5

Fitting	$r_s^{'1/2} C_{in}$	I_L'	A_α
14-Point	9.62×10^{-11}	2.0×10^{-14}	2.21×10^{-37}
5-Point	9.99×10^{-11}	2.31×10^{-14}	2.01×10^{-37}

The values of $r_s^{'1/2} C_{in}$ obtained are within a few percent from the mean obtained from the 'time' domain measurements. It is to be noted that values for such a parameter could be obtained more directly with an instrument not limited to 20 KHz, so that the flat part of the spectrum could be sampled more easily.

Using the 14-point results, the three different noise components have been calculated as a function of frequency and are shown in Fig. 3. It is evident that an accurate reading of I_L' in opto-feedback systems with small parallel noise components requires careful measurements at frequencies lower than 250 Hz. There is no real problem in carrying this out but one must use very narrow bandwidth so as not to get false readings from hums due to the line frequency and its harmonics, plus some low frequency microphonic effects which are often noticed. These effects, although small, they can easily contribute many eV of noise at very long peaking times.

Table 6 finally shows the calculated noise line widths from the parameters measured in frequency domain for the longer peaking times. Equation (25) is used for this purpose and the relative noise power contributions of the three terms are shown. The results are plotted in Fig. 2 for a comparison with the 'time' domain measurements.

TABLE 6

τ_o	Parallel	Series	1/f	NLW(FWHM)
4.36	1.46×10^{-38}	1.15×10^{-35}	1.52×10^{-36}	202 eV
7.7	2.62×10^{-38}	6.45×10^{-36}	1.52×10^{-36}	157 eV
17.	5.75×10^{-38}	2.92×10^{-36}	1.52×10^{-36}	118 eV
34.	1.15×10^{-37}	1.46×10^{-36}	1.52×10^{-36}	98 eV
65	2.21×10^{-37}	7.61×10^{-37}	1.52×10^{-36}	88 eV
140	4.77×10^{-37}	3.53×10^{-37}	1.52×10^{-36}	85 eV

A slight discrepancy is observed between τ_o = 4 to 35 μs in which the calculated values of NLW are slightly higher than the experimental results. This is likely to be caused by some inaccuracy in determining $r_s'^{1/2}$ C_{in}, since measurements at the high frequency end were limited to 20 KHz by the instrument used.

The calculated NLW at τ_o = 140 μs is a few eV lower than the measured results. This is due to some remaining 60, 180, 240 and 300 Hz hums clearly observable in the noise frequency spectrum. As much as 10 eV of noise have been removed at τ_o = 140 μs, to arrive at the measured value of 91 eV FWHM, by turning the spectrum analyzer to 180 Hz and positioning a ground strap between two carefully selected points between the detector cryostat and the NIM bin so as to minimize the amount of hum in the spectrum.

It is evident from the shape of the curve of resolution vs τ_o, and from Table 6, that the spectrometer system as set up for these measurements is severely limited by the 1/f and/or f-type noises. If one assumes C_{in} = 5 pF, and that all the noise is series 1/f due to the FET, a constant $A_\alpha = 2.21 \times 10^{-37}$ corresponds to a constant $A = 1.76 \times 10^{14}$ as defined customarily[1,3].

B. Germanium System Design Experiments

The practical objective of this project has been the construction of a low-energy Ge X-ray spectrometer with the lowest possible noise line width utilizing presently available FETs and detectors with a useful area of approximately 20 mm^2. The NLW results shown in Fig. 2 for a Si system (90 eV FWHM) indicate that, if noise parameters can be held constant in the switch over to a Ge detector, it should be possible to approach a NLW of 70 eV FWHM by virtue of the lower value of $\bar{\varepsilon}$ for Germanium. Furthermore, since there is no clear understanding at this time about the specific nature of the remaining noise in the systems, the work reported below was directed to obtaining that understanding and to attempt to lower the NLW further.

1. Detector fabrication and characteristics:

Single groove detectors of dimensions shown in Fig. 4 have been fabricated from two n-type Ge crystals grown at LBL by W. Hansen[7]. Crystal 201 had an impurity concentration of $3\text{-}5 \times 10^{9}$ cm^{-3}, while crystal 311 had a concentration of $2\text{-}3 \times 10^{10}$ cm^{-3}. The choice of n-type has been made in order to minimize the effective thickness of the entrance window by having the highest fields at the surface barrier side of the device[8]. The choice of geometry has been made from a previous observation[9] that grooved detectors can support very high fields and have quite stable surface conditions. The mechanism of surface channel pinch off[10] appears to account for those desirable characteristics as is demonstrated from noise measurements below and from the observed fact that low leakage devices are obtained only when the distance between the groove bottom and the surface barrier is 0.5 mm or less.

Detector fabrication has followed standard practice at the Lawrence Berkeley Laboratory[11] with a shallow Li-diffusion and a Pd surface barrier. Etching is quenched with electronic grade methanol exclusively and no other surface treatments have been carried out before the Pd evaporation or after the final short etching.

Finished detectors have been mounted on a Boron Nitride module as described schematically in Fig. 4. Initial tests have been made in a totally heat shielded cryostat (except for a few small right angle pump out holes). Capacitance vs voltage characteristics for two detectors are shown in Fig. 5, as measured at 1 KHz. When the depletion layer, which extends from the Pd contact, reaches the bottom of the groove there is a rapid decrease in device effective area, as evidenced from the fast drop in capacitance at low voltages, (Det. 311-1.7). Thinning of the region between the groove bottom and the Pd surface to reduce leakage current results in a substantial change in the C-V characteristics, as shown also in Fig. 5. Leakage currents below 10^{-14} amps at liquid N_2

temperatures with bias of at least 500 to 800 V are obtained with some regularity. Successful detectors can then be 'transplanted' in their modules to opto-feedback cryostats without any substantial change in characteristics. Noise behavior will be discussed below. Detection line broadening and background performance for X-rays will be the subject of a separate study.

2. Effect of detector mount on noise:

The detector module described in Fig. 4 contains an insulator 'wheel' which is in actual contact with the gate wire. The effect on noise of the insulator material used for the wheel and of two alternative ways of supporting the detector is reported in this section. Please refer to Table 7.

TABLE 7

FET P-15

COLUMN	1	2	3	4	5	6
Detector	Si C_d = 1.2 pF	Si C_d = 1.2 pF	201-3.7, Ge fresh. C_d = 1.1 pF Te disk holder	201-3.7, Ge large Te strap holder	201-3.7, Ge Mylar Ribbon holder	201-3.7, Ge re-etched C_d = 0.99pF B.N. wheel holder
$r_s'^{1/2} C_{in}$	9.6×10^{-11}	7.5×10^{-11}	8×10^{-11}	9×10^{-11}	7×10^{-11}	6.5×10^{-11}
I_L'	2×10^{-14}	1.5×10^{-14}	8.5×10^{-14}	3.5×10^{-14}	4×10^{-14}	4.5×10^{-14}
A_α	2.21×10^{-37}	2.25×10^{-37}	2.5×10^{-37}	2.75×10^{-37}	2.75×10^{-37}	2.25×10^{-37}
Calculated res τ_o = 64 - 70 μs	88 eV Si	82.5 Si	76 eV Ge	75 eV	71.5 eV	67 eV
Measured res τ_o = 64 - 70 μs	91 eV Si	84 eV Si	Microphonics too high	Microphonics better	72 eV Ge	Not measured
C_{fb}, dielectric	0.128 pF, B. N.	0.125 pF, B. N.	0.104, B. N.	0.104, B. N.	0.104, B. N.	0.104, B. N.
Observations	'open' cryostat	'closed' cryostat I_D = 1.57 mA V_o = 4 V W_{heater} = .16 W	No heat shield at detector entrance face; other i.r. leaks	Be Shield, i.r. leaks plugged	5 eV hum subtracted	

The results of the first column are those reported earlier in this paper for a Si detector of 1.2 pF capacitance supported by a thin mylar strap. The FET used was labelled P-15 and it was mounted on a Boron Nitride mount as described elsewhere[12]. The same detector and FET were transferred to a new cryostat of closed configuration, i.e., with both elements mounted inside a cylindrical heat shield, with the top cover formed by the Boron Nitride plate of Fig. 4. After careful FET temperature, current and voltage optimization the results of the second column were obtained, with substantially improved resolution. The most significant change has occurred in the r_s' term mostly due to optimization of the FET working conditions, but possibly also due to lowered resistance to the n^+ contact of the detector by the use of a pad of Indium. The detector was still held with a very tight thin strip of mylar.

With this last measurement as a reference, a Ge detector (201-3.7) was then placed in the cryostat. The module configuration of Fig. 4 was used, with the insulator wheel made of thin Teflon, with radial fingers to reduce possible losses. The metal wheel support was not grounded. The system proved to be extremely microphonic, so that NLW readings were useless. Fitting from frequency domain data yielded the results of the third column of Table 7. The value of $r_s'^{1/2} C_{in}$ obtained compared well with that of column 2, I_L' went very high, and the A_α parameter did not change significantly (it is estimated that changes in the noise power parameters $(r_s'^{1/2} C_{in})^2$, I_L' and A_α of 10% or less are not necessarily meaningful). Placing a 0.013 mm Be window in front of the exposed entrance to the detector as a heat shield and plugging with In foil other infrared light leaks resulted in a decreased I_L' as shown in the fourth column. Also, for this measurement a large solid Te strap was used to replace the metal-insulator detector holder. The system was much less microphonic, but a few large peaks still appeared in the noise frequency spectrum, contributing quite substantially to the NLW. In Column 5 the results of using a thin tight mylar strap are shown. The system was found to be very free of microphonics and the calculated and measured NLWs agreed very well. Finally, the metal insulator arrangement of Fig. 4 was used again, this time with a Boron Nitride wheel of about 1 mm thickness at the flat section, with results given in Column 6 of Table 7. The system was also quite free of microphonics. Subsequent measurements were carried out with this support arrangement with negligible microphonics effects, provided that the stainless steel wire (0.25 mm dia.) from the detector was not tensioned against the gate lead from the FET package.

Throughout this process, the $r_s'^{1/2} C_{in}$ term behaved quite erratically and this fact, supported further in the following sections, indicates that the manner of making contact to the Li-diffused region of the Ge detector is important and may account for four or more eV of noise. A eutectic Ga-In mixture has been used on the Li-contact in all the measurements with the B. N. wheel.

The I_L' term is extremely sensitive to IR radiation seen by the detector. Some evidence shows that the FET package (hotter than the surroundings) is 'seen' by the detector. There is, however, no problem with I_L' as its contribution to NLW is comparatively quite small if it is kept at or below 3×10^{-14} Amps. During the measurements it was observed that recycling the cryostat to air repeatedly resulted in a slow, but steady increase in I_L'. For the measurement of Column 6, the detector had to be re-etched, but in this particular case I_L' still remained somewhat high. Usually, refabricating the surface barrier and re-etching brings back values of I_L' in the region of 2×10^{-14} Amps.

The A_α term has remained between 2.25×10^{-37} and 2.75×10^{-37} for both the Si and the Ge detector. A discussion regarding the origin of this noise will be given below. At this time, however, one can state that no significant effect on A_α has been noticed by any of the detector mounting materials tested. Furthermore, grounding the metal wheel support only modified the $r_s'^{1/2} C_{in}$ parameter in measure of the increased C_{in} with no effect on A_α, indicating that insulator losses due to the cold B. N. wheel were negligible.

Another observation that should be mentioned at this point is that 60 Hz hum, with its odd harmonics, made its appearance quite strongly during the measurements of Table 7. The figure for measured resolution of 72 eV of Column 5 was arrived at by substracting in quadrature the amounts of 60, 180 and 300 cps signals measured by the spectrum analyzer from the RMS meter noise readings. NLW reduction was from 77 to 72 eV FWHM. In subsequent measurements with the same cryostat the hum problem was solved by placing a 1000 pF ceramic capacitor between the H. V. wire feeding the detector and the source of the FET inside the cryostat, thus providing a by-pass for currents induced in the cryostat walls which otherwise would flow through the detector-FET circuit. With this arrangement hum contributions have been reduced to less than 1 eV at $\tau_o = 70$ µs.

3. Effect of Boron Nitride FET mount:

An initial qualitative examination of the behavior of the three noise parameters as a function of FET package temperature was carried out by warming up the FET package with a fixed heater power for a certain length of time and making measurements at five frequencies (one frequency per run) as the FET was allowed to cool. This was done for FET P-15, with the same Si detector used previously. This temperature runs were made several times under different V_D and I_D conditions for the FET and the general qualitative picture which emerges is shown in Fig. 6. The $(r_s' C_{in}^2)^{1/2}$ term increases substantially with lowering temperature; I_L' remains essentially constant and the A_α term is high when the FET is too hot, goes through a minimum upon cooling and then increases quite rapidly upon further cooling. The point of

optimum NLW at long τ_o is then determined almost exclusively by the A_α constant, and in fact, a non-microphonic system can be optimized by minimizing the RMS noise at a frequency of 2 KHz, for example.

A microphonic system may have a different NLW optimum, as microphonics of a kind which occurs in the region of a few KHz decreases strongly at increased temperature (FET Kovar lead?).

Observation of Fig. 6 seems to indicate the possibility of two mechanisms causing the behavor of A_α, one with decreased influence at lowered temperatures and one which increases A_α and possibly $r_s'^{1/2} C_{in}$ with decreasing temperature, in such a way that a minimum of noise is attained. In this section, the possibility that the remaining 1/f noise at the optimum temperature is caused by the amount of B. N. in contact with the gate lead is investigated.

A FET which had been very carefully selected for low noise at long τ_o, labelled 66X-F, was placed in the test cryostat, along with the refabricated detector 201-3.7. Measurements in frequency domain (12-points) were carefully made and NLW was then calculated and measured at τ_o = 70 μs. The results appear in the first column of Table 8. Next the FET was removed from its B. N. mount and placed in a new mount which had been modified by removing a cylindrical portion of material around the gate wire. This is shown schematically in Fig. 7. The feedback capacitance wire was placed in hole A, Fig. 7, as previously--but was not pushed in more than half way. The results of the measurements with the new package are shown in Column 2 of Table 8. Figure 8 shows the frequency domain results, with the fitted functions. The vertical scale for this figure and similar forthcoming ones is normalized to a C_{fb} = 1×10^{-13} pF for uniformity of presentation. It appears that the modified mount may have resulted in a decrease of the A_α parameter. The magnitude of this decrease is, however, too small to be certain.

From this measurement one can then conclude that at the optimum temperature of operation, removing more than one half of the B. N. in contact with the gate lead may provide at best an almost inmeasureable improvement in the A_α parameter.

TABLE 8

FET 66X-F

COLUMN	1	2
Detector	201-3.7, reprocessed C_d = .9 pF B.N. disk holder	201-3.7 C_d = .9 pF (system open for 48 hrs.)
$r_s'^{1/2} C_{in}$	8.5×10^{-11}	8.5×10^{-11}
I_L'	2.5×10^{-14}	2.1×10^{-14}
A_α	2.75×10^{-37}	2.4×10^{-37}
Calculated res τ_o = 70 μs	72.8 eV Ge	69 eV
Measured res τ_o = 70 μs	72 eV Ge	73 eV Ge
C_{fb}	.1 pF B.N.	.043 B.N.
Observations	I_D = 3 mA V_D = 4 V W_h = .128 W	Modified mount

4. Effect of feedback capacitor dielectric:

If the noise due to dielectric losses can be adequately represented by the formulation of Radeka[3], then its contribution should be largest between points with highest capacitance, i.e., between the FET gate and the C_{fb} wire imbedded in the Boron Nitride mount. To check on this possible noise source several tests have been carried out, with results on Table 9.

FET 66X-F in its modified mount and detector 201-3.7 were again used for these tests. Two measurements with the C_{fb} wire in position A, Fig. 7, with different depths of insertion were first made. Next the wire was inserted in position B, with the tip of the wire very near the gate wire in vacuum and another set of measurements was made. The frequency domain results are shown in Fig. 9. It is evident that the three measurements give indistinguishable results. A range of A_α values has been plotted to indicate the accuracy of the measurement. Fitting parameters appear in Columns 1 and 2 of Table 9. It is believed that the large value of $r_s'^{1/2} C_{in}$ in those results is due to n^+ contact deteriozaation with repeated system temperature cycling and baking to reduce detector leakage.

TABLE 9

COLUMN	1	2	3
FET	66X-F Modified Mount	66X-F Modified Mount	T-29
Detector	201-3.7(x)	201-3.7	Small Si $C_d = 0.35$ pF
$r_s'^{1/2} C_{in}$	1×10^{-10}	1×10^{-10}	6.2×10^{-11}
I_L'	4×10^{-14}	4×10^{-14}	8×10^{-15}
A_α	2.5×10^{-37}	2.5×10^{-37}	2.25×10^{-37}
Calculated res, $\tau_o = 70$ μs	74 eV Ge	74 eV Ge	78 eV Si
Measured res $\tau_o = 70$ μs	71 eV	77.5 eV (microphonics at f > 20 Kc?)	77 eV Si
C_{fb}	.078 B.N. and .062 B.N.	.082 Vacuum	.078 Teflon
Observations	(x) system open to air 4 times, baked to 60°C twice for 24 hrs.		

The next measurement was made on a different system with a very small Si detector and FET (T-29) with a Teflon cylinder inserted in an aperture similar to the one of Fig. 7 in such a manner that Teflon is the main C_{fb} dielectric. Column 3, Table 9, contains the parameters observed. This system is one of the best made at LBL for large τ_o operation.

It is quite evident from Table 9 that no important change has occurred to A_α from the changes in dielectric. It is possible that the reduction of 2.5 to 2.25×10^{-37} observed in going from Ge to Si may be significant (Table 7 also seems to show such an effect), but it could be due, in this case, to lower C_{in}.

We conclude from this section, that the value of $A_\alpha \simeq 2.5 \times 10^{-37}$ observed regularly is not primarily due to feedback capacitor dielectric effects.

5. Searching for the origin of 1/f noise:

Since it is quite evident from the above results that the primary source of 1/f noise at optimum operating temperature is not insulator losses, an attempt has been made at determining the dependence of A_α on C_{in} and FET package operating temperature with the hope of determining whether the detector or the FET is the main source. Bearing in mind that the parameter A_α is defined as

$$A_\alpha = (A_s/2)\, C_{in}^2 + (A_{sd}/2)\, C_d^2 + (A_f/2) \qquad (52)$$

from Eqs. (25) and (46), one could expect that varying C_d by changing detector voltage might make it possible to determine which of the terms of Eq. (52) is the dominant one.

0 0 ⌄ 4 3 0 1 4 6 3

Measurements were carried out with detector 201-3.7 in a good surface condition ($I_L' \approx 2.2 \times 10^{-14}$) and FET 66X-F. Twelve-point measurements in frequency domain were made at a variety of FET heater power settings such that A_α ranged from too high, to optimum, to too high again (Fig. 6), with detector capacitances ranging from 0.88 to 2.7 pF. At higher values of C_d, A_α became so large that the other two parameters could no longer be estimated with any accuracy. The measurements will be discussed in two parts: 1) at optimum temperature and progressively higher (TOPT,TOPT+,TOPT++) and 2) at optimum temperature and progressively lower (TOPT,TOPT-,TOPT--,TOPT---).

Figure 10 shows I_L' vs C_d at three settings of temperature. As detector capacitance increases, parallel noise is seen to increase, with no clear dependence on FET temperature. The only plausible explanation that can be given for this effect is that, at low detector bias, resistive noise generated in the surface channels, coupled to the circuit by a channel-to-bulk capacitance, contributes parallel noise. A channel resistance of 10^{11} Ω, coupled by 1 pF could account for the magnitude and frequency of the effects observed. At higher bias, the surface channels deplete, leaving the parallel noise due primarily to leakage current.

Figure 11 shows the values obtained for $r_s'^{1/2} C_{in}$ as a function of C_d and temperature. With a well depleted detector, an improvement in the parameter is noticed with increased temperature, corresponding to the qualitative results of Fig. 6. At detector bias below depletion the increase in the series noise component is much larger than what is expected by the increase in C_{in}. It is quite clear that the series resistance of the undepleted germanium is adding noise to the system.

Figure 12 a) shows the results for A_α obtained in the same set of measurements, plotted as a function of C_d. With the value of $C_{in} = C_d + 3$ pF for a 2N4416 FET out of its can, A_α has also been plotted as a function of C_{in} in Fig. 12 b). If we assume that the contribution to A_α by the detector is constant, or at least does not increase with lowering bias below depletion voltage, the graphs of Fig. 12 can be interpreted by the use of Eq. (52). It becomes apparent that A_α is closely proportional to C_{in}^2 at the temperatures tested indicating that the noise appears as a series source at the FET, as would be the case for channel surface noise[13]. Furthermore, there does not seem to be any substantial parallel insulator loss contribution (A_f) to A_α, which is in agreement with the findings reported in previous sections.

In order to discuss the FET behavior at temperatures below the optimum, please compare Figs. 13 and 14 containing frequency domain data taken at TOPT and at TOPT---. Although it is clear that the three parameter model of Eq. (47) can be used to fit the experimental results at TOPT (solid lines, Fig. 13), such a model would not fit the results at the lower temperature because of the appearance of a step at $f \approx 5$ KHz.

Sah[14] has shown in his theory of low frequency generation noise in FETs that the predominant noise source due to trapping centers is due to generation in the gate-junction transition region, particularly at low temperatures. The equivalent frequency dependent noise resistance due to such an effect can be given as

$$r_g = K \frac{1}{3kT} \frac{\tau_t}{(1+\omega^2 \tau_t^2)} \qquad (53)$$

where K is a constant depending on material and device parameters and τ_t is a temperature dependent generation time constant defined as

$$\tau_t = \frac{1}{\sigma_p v_t p_1 + \sigma_n v_t n_1} \qquad (54)$$

where $p_1 = N_V \exp(-(E_t - E_V)/kT)$, $n_1 = N_C \exp(-(E_C - E_t)/kT)$, σ_p and σ_n are capture cross sections and v_t is thermal velocity. E_t is trap energy.

Since the noise dependence on frequency observed in Fig. 14 strongly suggests the presence of a term of the form of Eq. (53) added to our previous noise model (Eq. (47)), a new fitting has been made to the data obtained at four temperatures between TOPT and TOPT---, with a fully depleted detector, using a function of form

$$Z(f) = \left[(a_1/f^2) + (a_2/f) + a_3 + a_4 \frac{\tau_t}{1+\omega^2 \tau_t^2}\right]^{1/2} \qquad (55)$$

with a_1 to a_3 defined by Eqs. (48) to (50) and a_4 by

$$a_4 = K_g (C_{in}/C_{fb})^2 \qquad (56)$$

where K_g is a temperature independent constant. The results of the new fitting appear in Fig. 15.

Constants a_1 to a_3 were evaluated from noise parameters at TOPT and kept fixed. The curve for TOPT--- was used to obtain the best values for a_4 and τ_t and then, keeping a_4 fixed, new values of τ_t were found for the other curves. The results of the fitting appear in the figure. The value of $K_g C_{in}^2$ used was 5.5×10^{-35}

The results obtained for τ_t can be interpreted with the aid of Eq. (54). Since τ_t is small compared to values corresponding to deep traps[14], one can assume that the trapping center involved is not very deep, in which case either n_1 or p_1 can be neglected. Then, with

$v_t = 10^7\ (T/300)^{1/2}$ cm/sec one can calculate the locus of values of σ_n (for example) and E_t such that a given value of τ_t will be satisfied at a given temperature. Figure 16 shows three such lines, one each for the values of τ_t obtained in the data fittings at different experiment temperatures. After arbitrarily deciding that TOPT--- may have been 90°K, it is found that σ_n and E_t are almost uniquely defined if TOPT-- is equal to 100°K and TOPT- is 110°K, a very plausible result. This uniqueness still holds approximately for any other reasonable choice of temperature TOPT---. For σ_n ranging between 10^{-15} and 10^{-13} cm^2, which covers a wide range of the trapping cross sections published[15], it seems that E_t may be between .11 and .16 eV. This measurement alone cannot be used, however, to obtain information about the traps beyond the realization that they are deeper than shallow donors or acceptors, but not as deep as Au.

The good fitting shown in Fig. 15 and the plausibility of the temperature range shown in Fig. 16 lend support to the modified noise model of Eq. (55) and to the statement that the apparent increase of A_α and $r_s'^{1/2}\, C_{in}$ at temperautres below optimum are due, instead, to generation due to traps in the gate junction depletion layer.

V. CONCLUSIONS

The value of frequency domain analysis of noise sources has been amply demonstrated, particularly in the identification of noise sources with substantial intensity variations in the frequency domain over bandwidths which are narrow in comparison with standard nuclear spectrometry filters, as are microphonics, hum and the gate junction recombination noise. The analysis in frequency domain can be made totally quantitative and spectrometric noise line widths can be predicted with the accuracy with which one can read oscilloscopes and meters. Frequency domain analysis carried out with a standard sweeping heterodyne instrument is quite slow, however. A 12-point analysis takes approximately 30 minutes for data taking with the accuracies used in the present work, plus 15 minutes for interactive computer analysis. This is very acceptable for occasional work, but a more modern instrument ('real time' analyzer) would be needed for a serious program, as in low noise FET development work.

From the practical point of view of low noise spectrometer design, it has been shown that the 28% improvement in NLW expected by switching from Si to Ge detectors is fully realizable. Low leakage devices can be made with some regularity, they do not usually contribute substantial 1/f noise of their own (one detector did raise A_α to 5×10^{-37} in one instance), and once properly mounted they require only elementary Ge detector care.

Detector and FET mounts made with high-quality boron nitride have been shown to contribute no substantial amount of noise, and the use of that material as dielectric for feedback capacitors is perfectly acceptable. Hums can be brought under control by proper circuit wiring and by-passing, but microphonics is a complex problem which we have managed to control well in only one cryostat, so far (short cold finger, vertical configuration dip stick).

The finding that the FET noise behavior at long peaking times is limited at the higher operating temperatures by its own surface noise and at the lower by trap generation noise places the emphasis of any further low-noise preamplifier development on the FET manufacturing processes, with particular attention to the presence of trapping centers and surface state control.

VI. ACKNOWLEDGEMENTS

The author is very grateful to F. S. Goulding for considerable support and very valuable discussions, to D. A. Landis, N. W. Madden, and R. C. Cordi for contributing some of their very valuable experience to the project and to D. F. Malone for the fabrication of the detector mounts.

REFERENCES

1. R. Benoit, Semiconductor Detectors, Bertolini and Coche, Eds., Wiley, Sec. 3.1 (1968).
2. F. S. Goulding, Nucl. Instr. and Meth. 100, 493 (1972).
3. V. Radeka, Int. Symp. on Nuclear Electronics, Versailles, France, (Sept. 1968).
4. V. Radeka and N. Karlovac, Nucl. Instr. and Meth. 52, 86 (1967).
5. V. Radeka and N. Karlovac, Semiconductor Radiation Detectors and Circuits, Nat. Acad. Sci. Publ. 1593, 553 (1969).
6. A. D. Whalen, Detection of Signals in Noise, Academic Press, N. Y. Secs. 4.3 and 4.5 (1971).
7. W. L. Hansen, Nucl. Instr. and Meth. 94, 377 (1971).
8. F. S. Goulding, R. H. Pehl, private communication.
9. J. Llacer, Nucl. Instr. and Meth. 98, 259 (1972).
10. J. Llacer, IEEE Trans. Nucl. Sci. NS-13, No. 1, 93 (1966).
11. R. H. Pehl, R. C. Cordi and F. S. Goulding, IEEE Trans. Nucl. Sci. NS-19, No. 1, 265 (1972).

12. F. S. Goulding, J. T. Walton and D. F. Malone, Nucl. Instr. and Meth. 71, 273 (1969).

13. A. Van der Ziel, Noise, Prentice-Hall, Sec. 6.4 (1970).

14. C. T. Sah, Proc. of the IEEE, 52, 795 (1964)

15. A. G. Milnes, Deep Impurities in Semiconductors, Wiley, Sec. 10.6 (1973).

FIGURE CAPTIONS

Fig. 1. Equivalent circuit for the noise sources in a detector-preamplifier system.

Fig. 2. Noise line width (FWHM) vs peaking time for a moderately good Si(Li) X-ray spectrometer system, comparing direct measurement results with calculated results from frequency domain measurements.

Fig. 3. Preamplifier output noise spectrum for the same Si(Li) system of Fig. 2, showing the three individual components of Eq. (47).

Fig. 4. Schematic drawing of single groove Ge detector and its mount.

Fig. 5. Capacitance vs voltage characteristics of two n-type Ge detectors, showing rapid drop in capacitance when the depletion layer reaches the bottom of the groove. (Det. 311-1.7).

Fig. 6. Qualitative behavior of system noise parameters as a function of cooling time from FET temperature higher than optimum. See text for correct interpretation.

Fig. 7. Schematic drawing of Boron Nitride FET mount indicating some modifications tested.

Fig. 8. Normalized frequency domain data of Ge detector system showing effect of removing 50% of Boron Nitride in contact with gate lead. Apparent improvement is too small to be considered reliably true.

Fig. 9. Normalized frequency domain data of Ge detector system showing effects of different feedback capacitor configuration. Sensitivity of the fitting to values of A_α is also shown.

Fig. 10. Behavior of the parallel noise term I_L' with variations of detector capacitance obtained by changing bias voltage on the high-purity Ge detector. Measurements at optimum FET temperature and above.

Fig. 11. Behavior of the series noise term $r_S'^{1/2}\,C_{in}$ with variations of detector capacitance. Measurements at optimum FET temperature and above.

Fig. 12. Behavior of the 1/f parameter A_α with variations of detector capacitance. Measurements at optimum FET temperature and above. a) A_α vs C_d; b) A_α vs C_{in}, defined as C_d + 3 pF for a 2N4416 FET out of its can. A line proportional to C_{in}^2 is shown in b) for comparison.

Fig. 13. Normalized frequency domain data for Ge system at optimum temperature, showing experimental and fitted points at different values of detector capacitance.

Fig. 14. Normalized frequency domain data for Ge system at the lowest temperature tested, showing experimental points with a step at about f = 5 KHz, for different values of detector capacitance.

Fig. 15. Normalized frequency domain data for Ge system at optimum temperature and below, fully depleted detector, showing the fitting lines and parameters for the Sah model of gate junction trap generation noise.

Fig. 16. Loci of σ_n and E_t consistent with trapping time constant τ_t fitted at three temperatures below optimum, showing uniqueness of σ_n and E_t if those temperatures are each separated by 10°K.

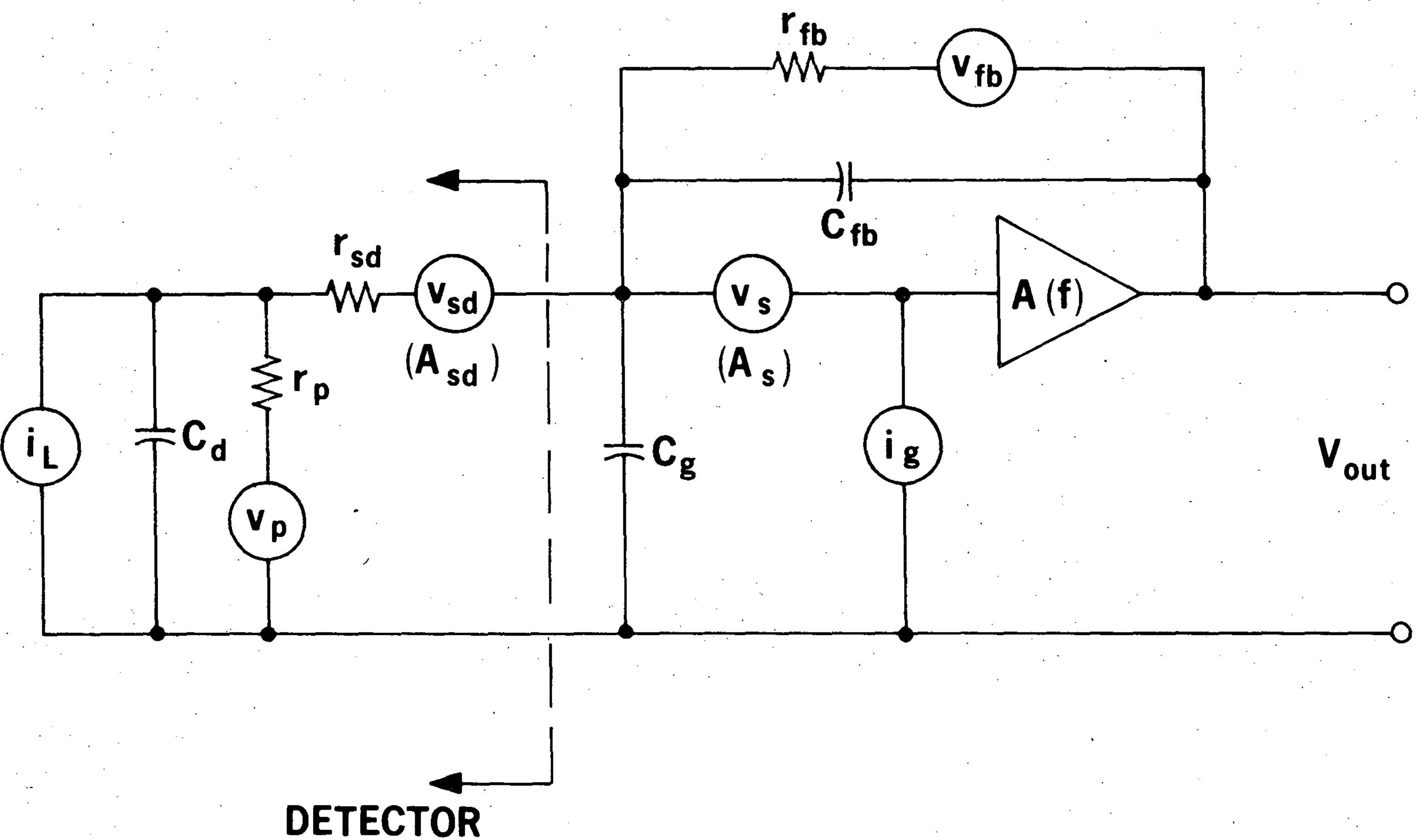

Fig. 1

XBL 751-22

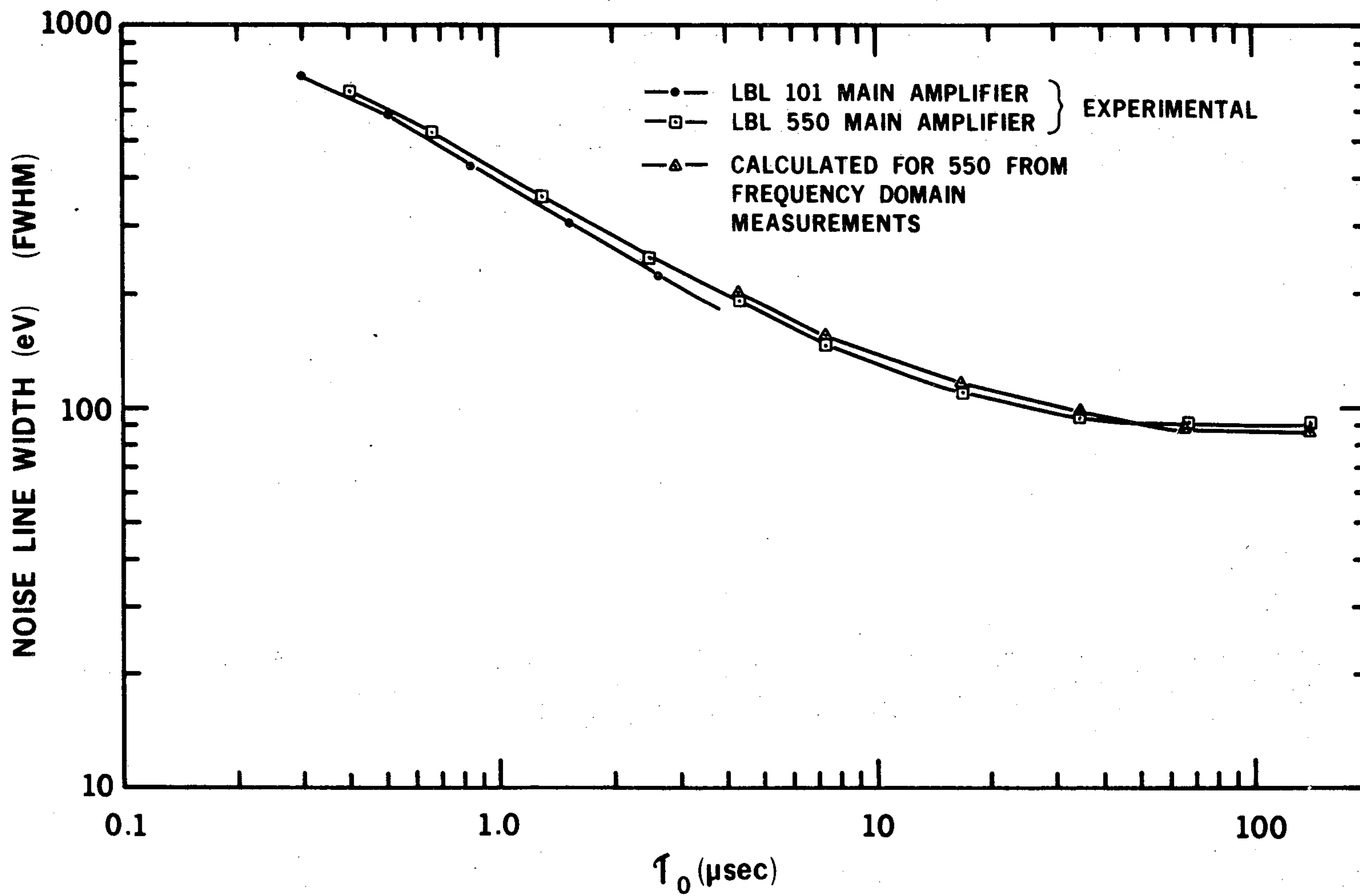

XBL 751-23

Fig. 2

0 0 0 4 3 0 1 4 6 5

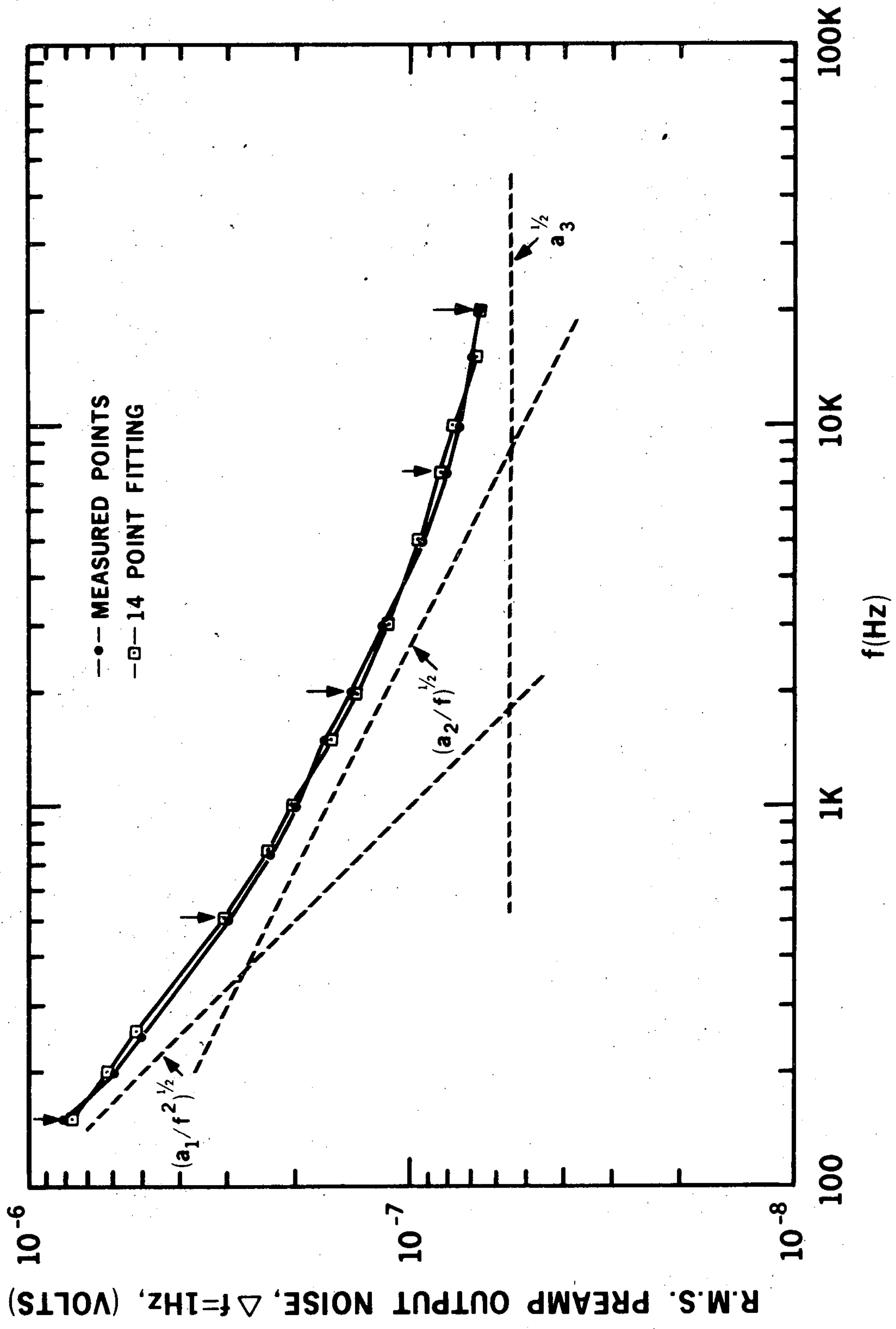

XBL 754-865

Fig. 3

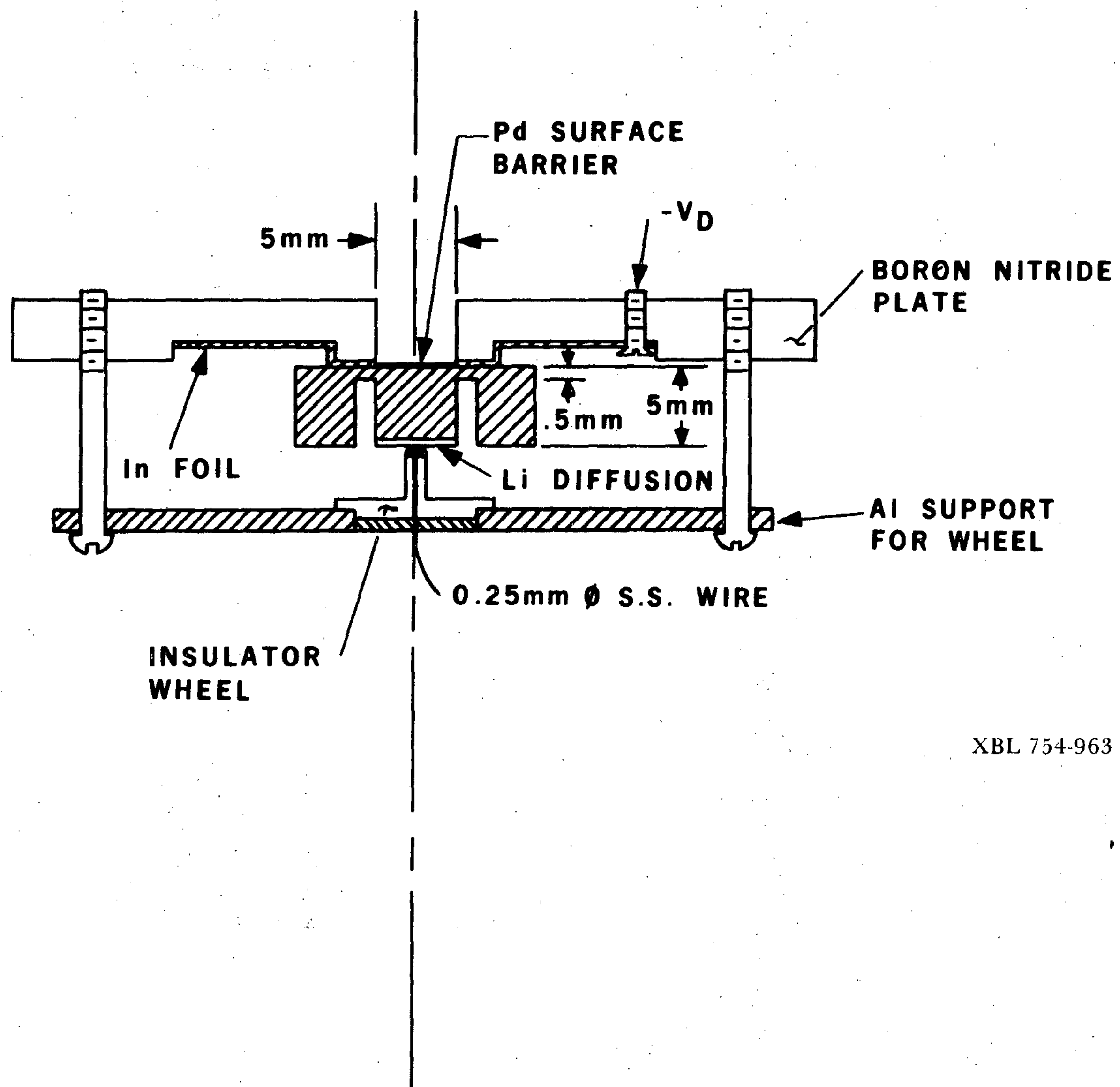

Fig. 4

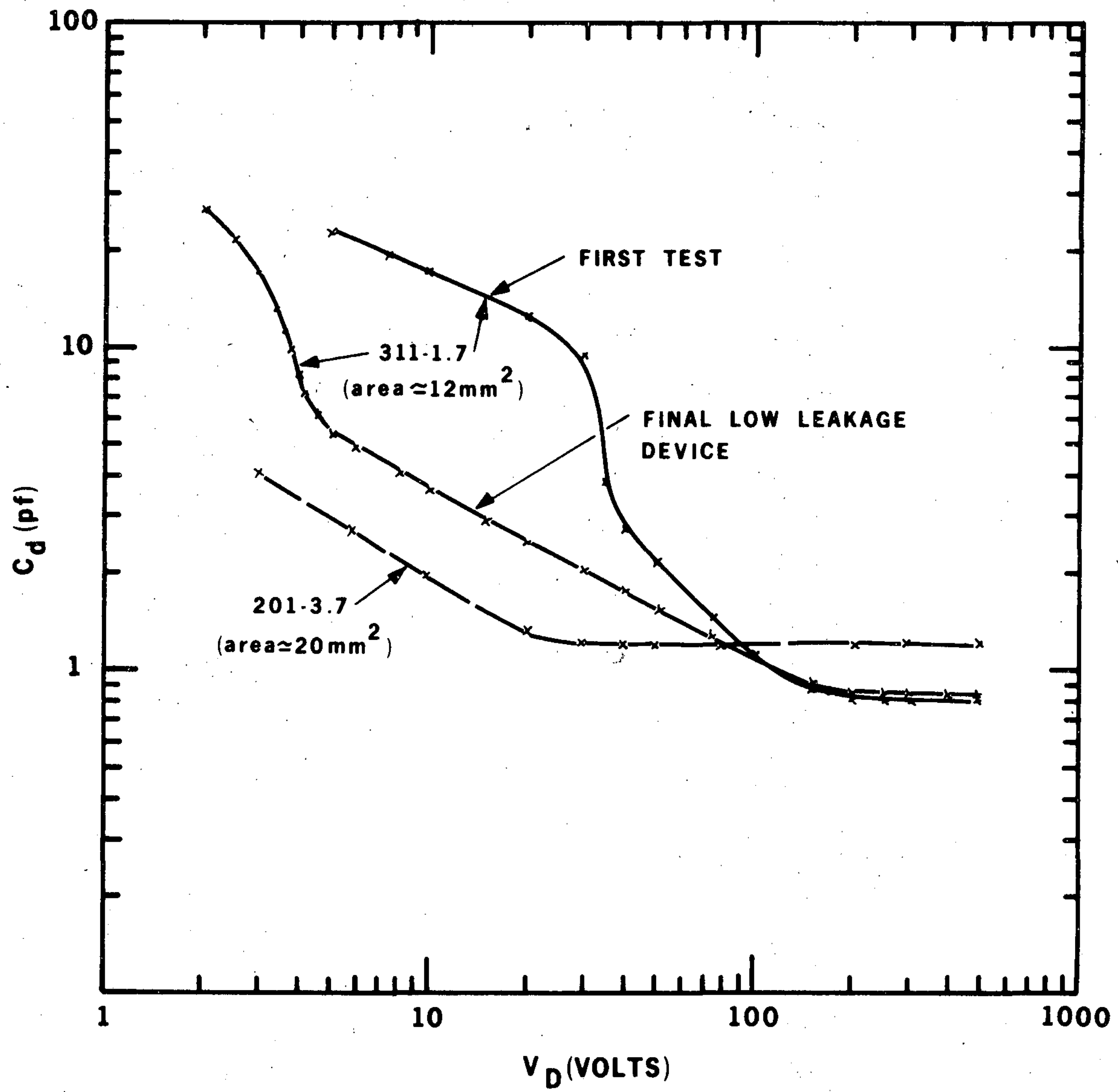

Fig. 5

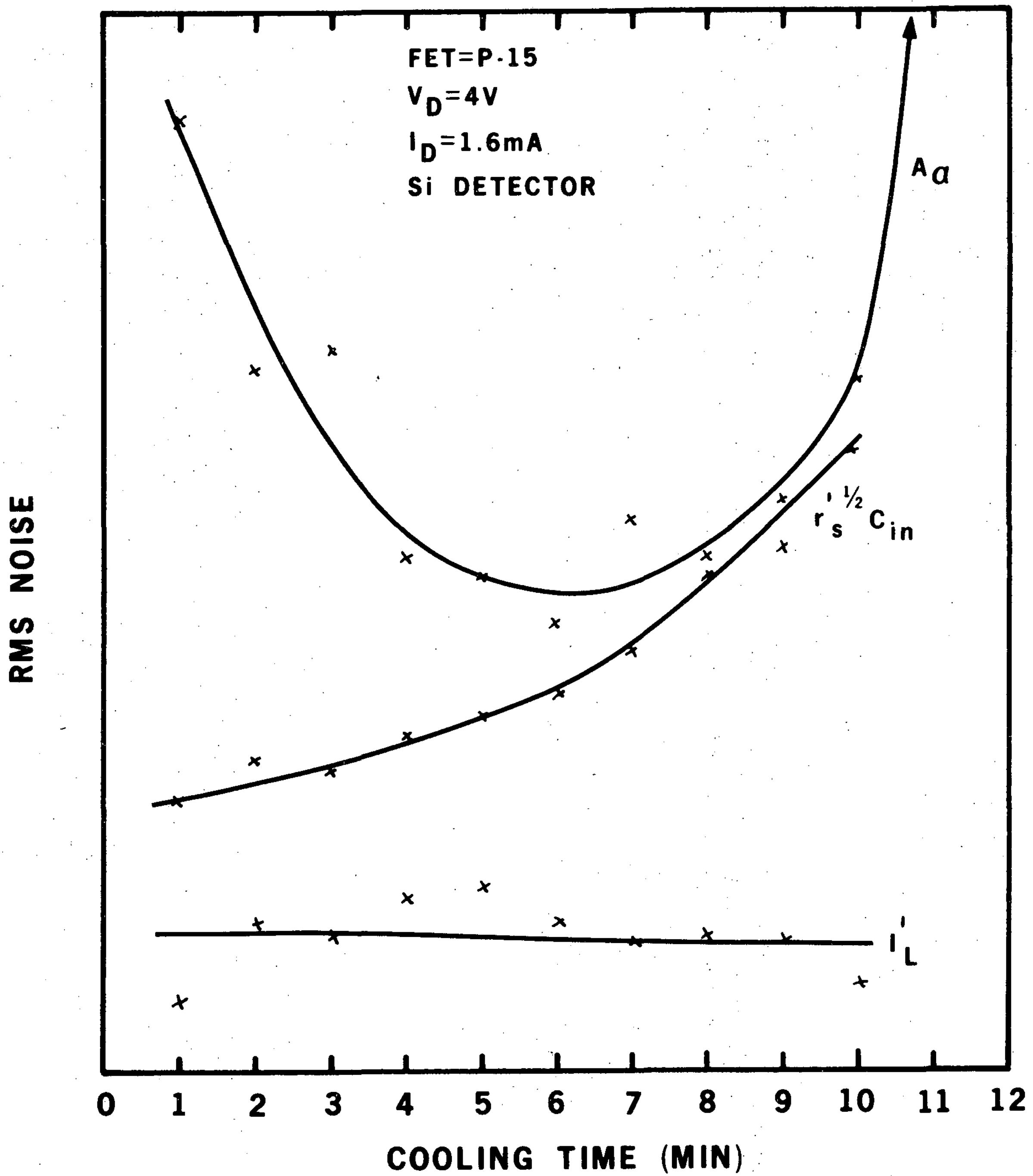

XBL 754-959

Fig. 6

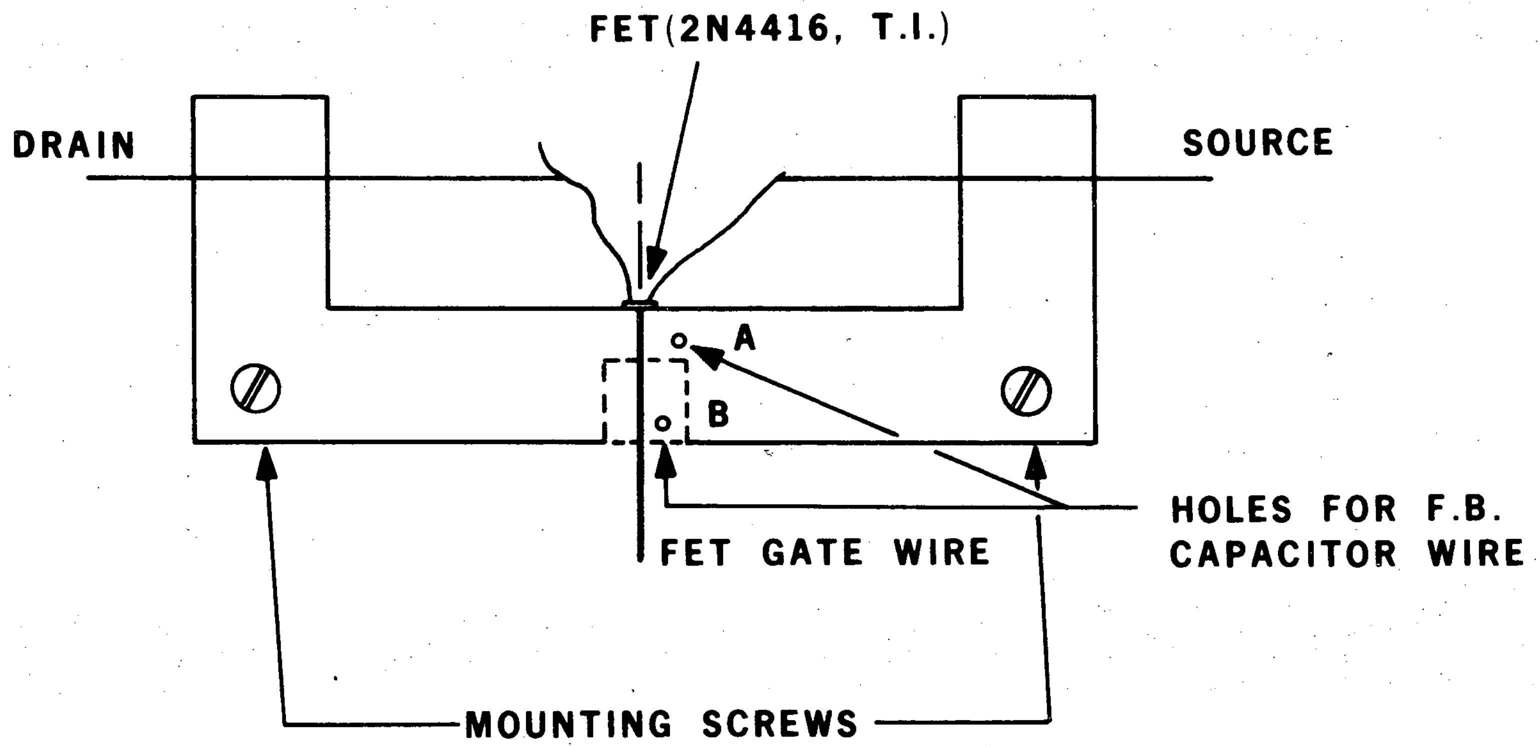

XBL 754-964

Fig. 7

0 0 0 4 3 0 1 4 6 7

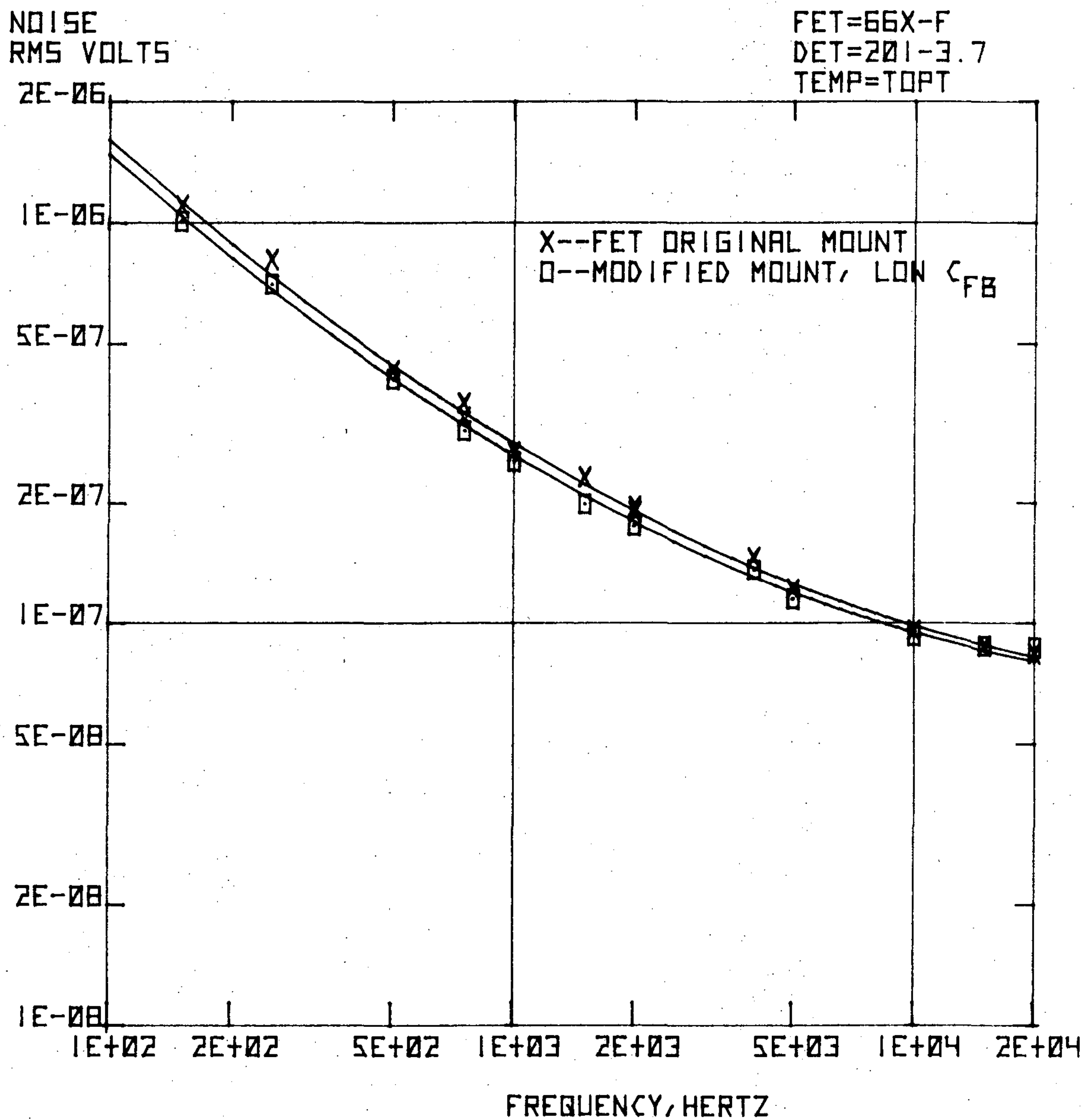

XBL 754-955

Fig. 8

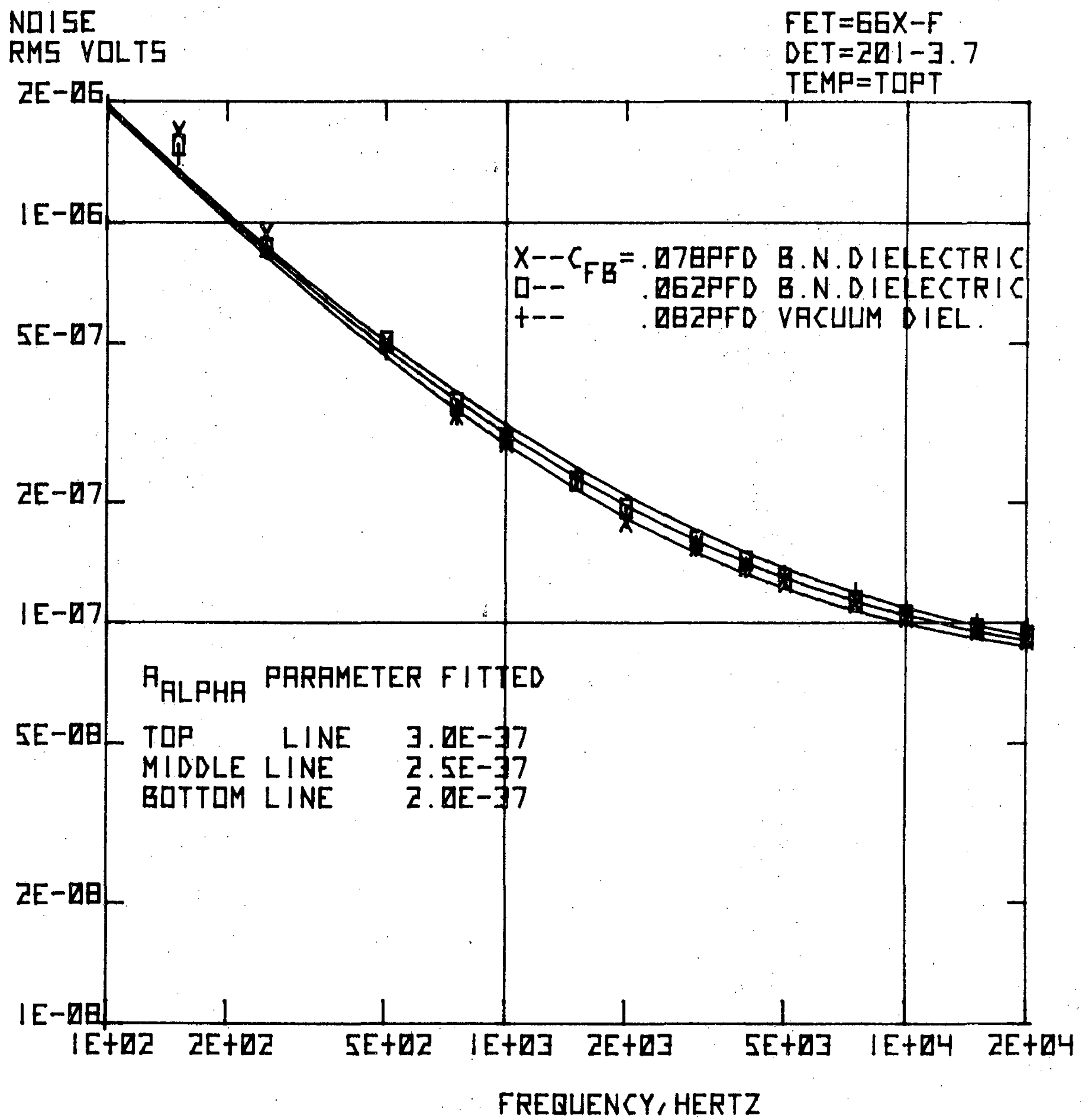

XBL 754-956

Fig. 9

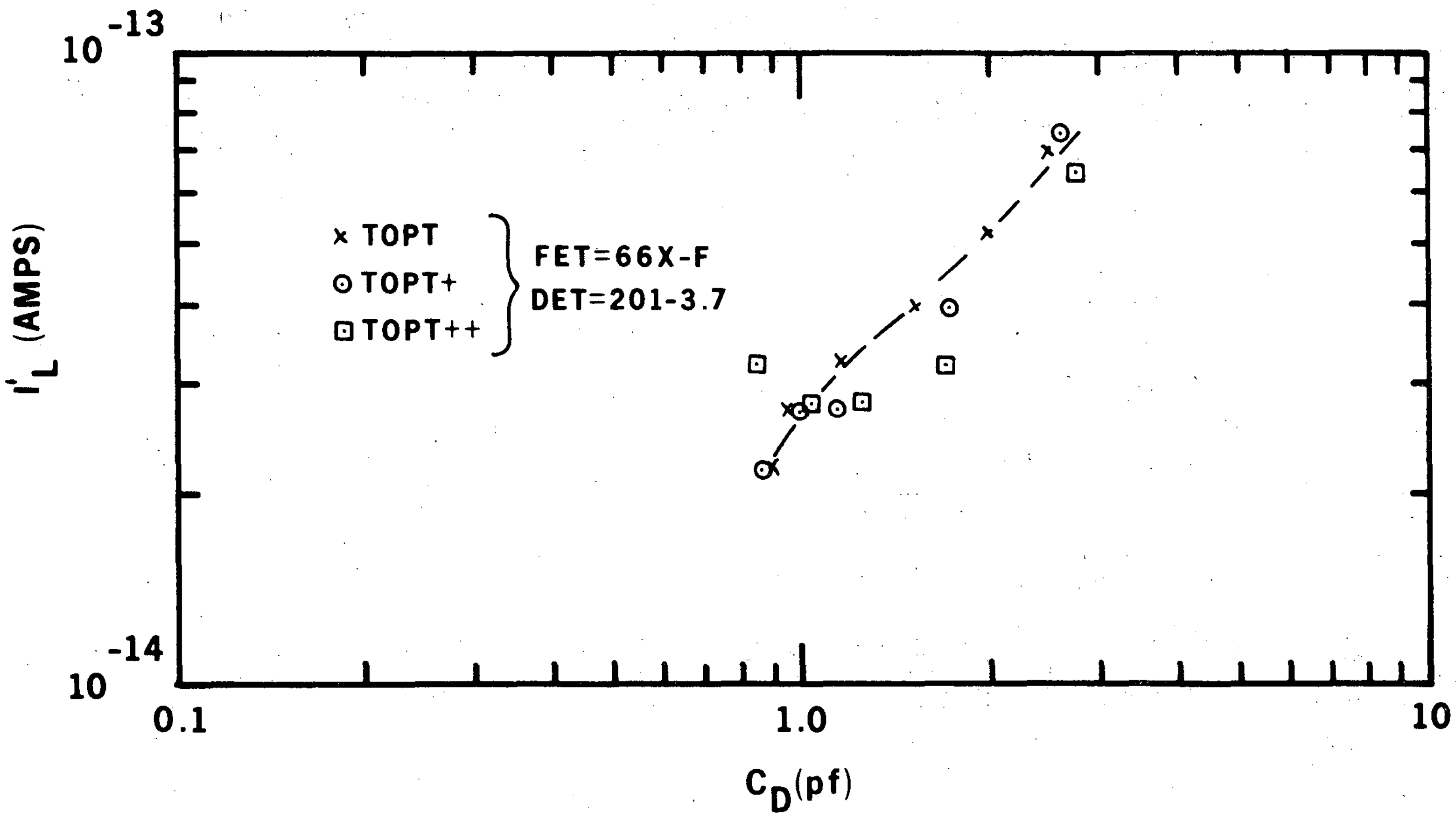

Fig. 10

0 0 0 4 3 0 1 4 6 9

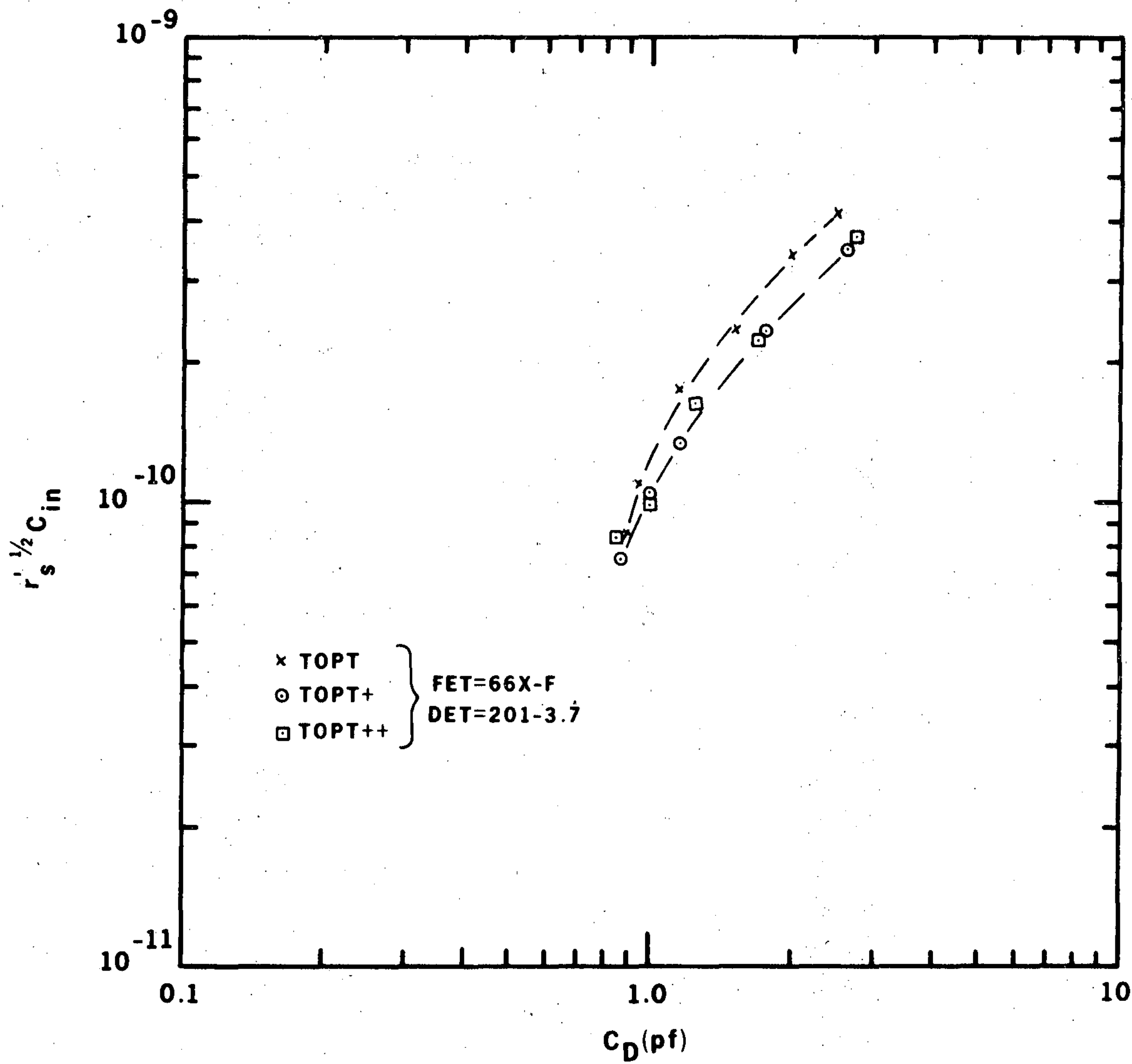

Fig. 11

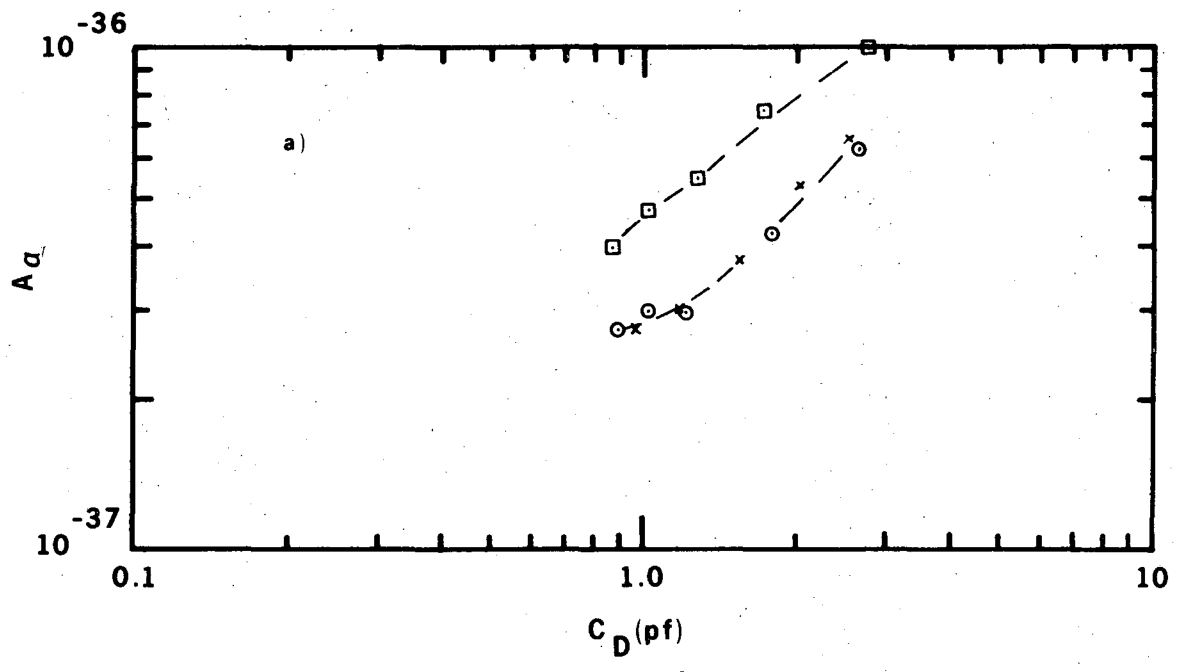

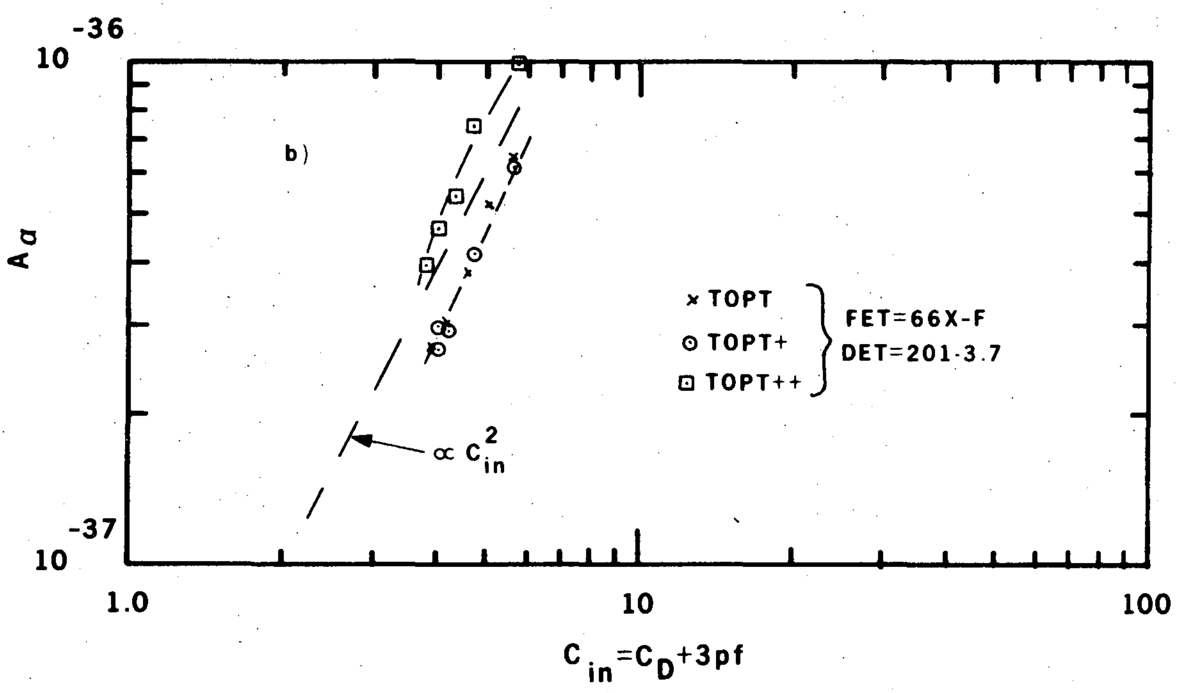

XBL 754-1002

Fig. 12

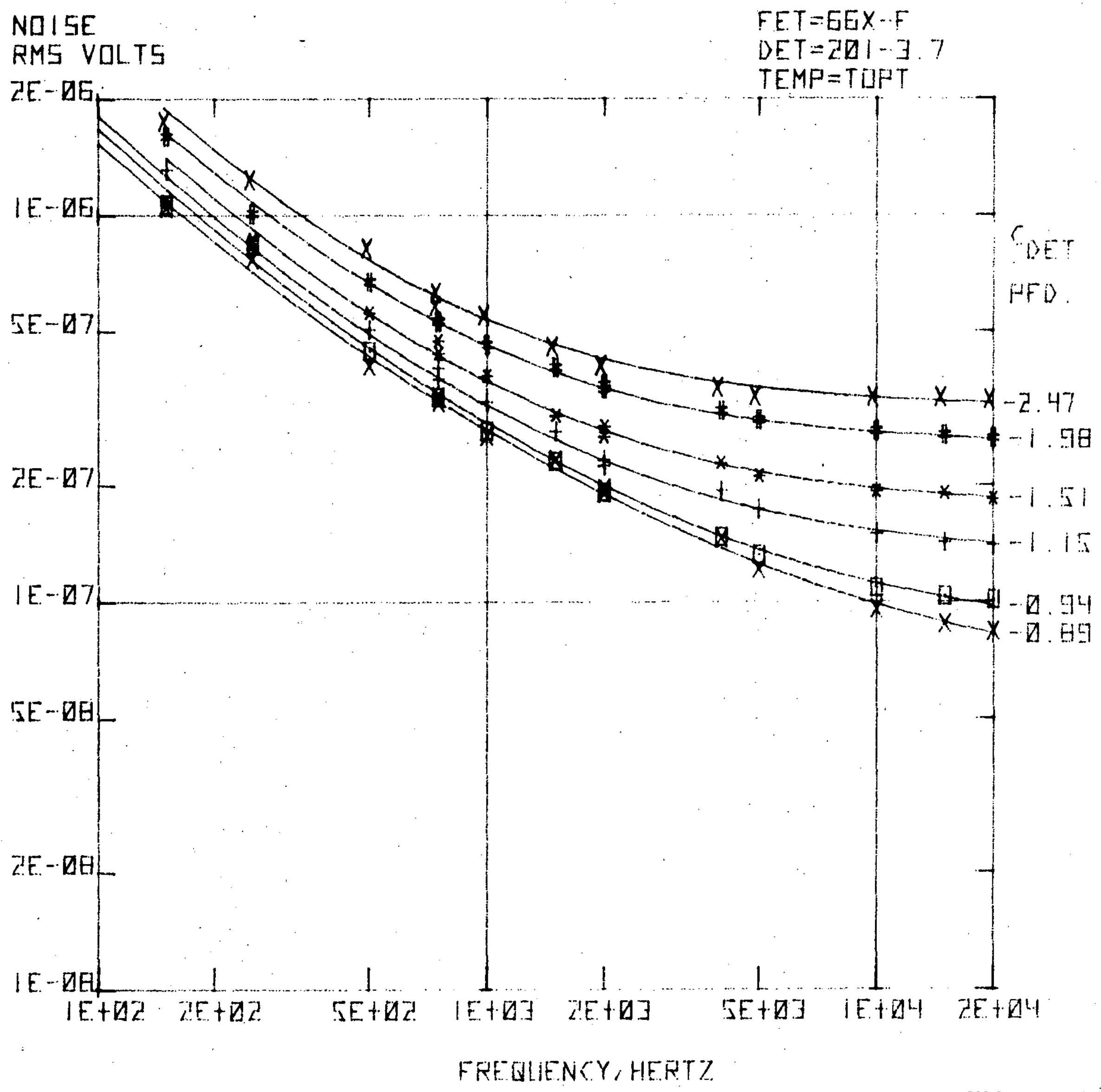

Fig. 13

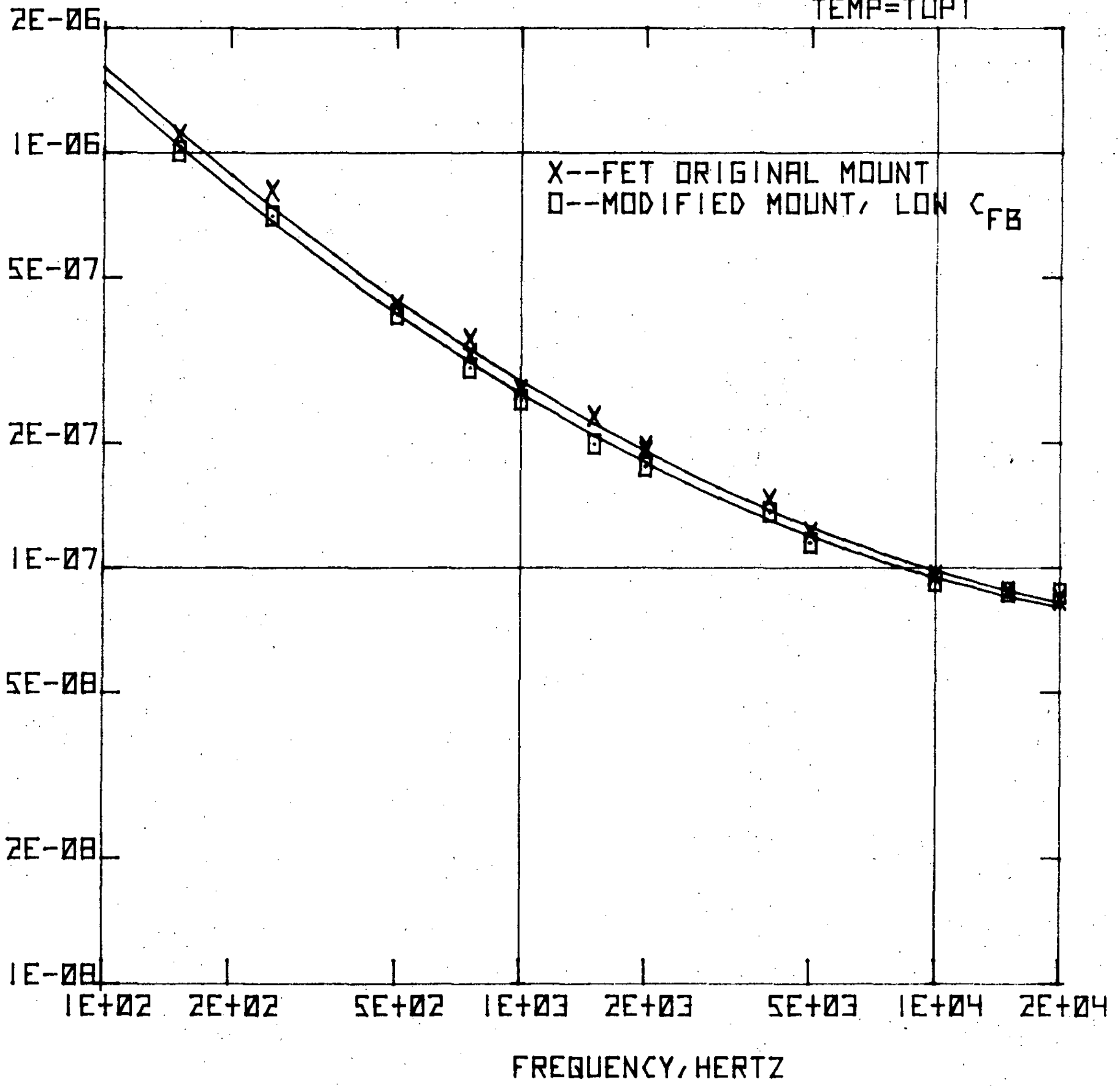

XBL 754-955

Fig. 14

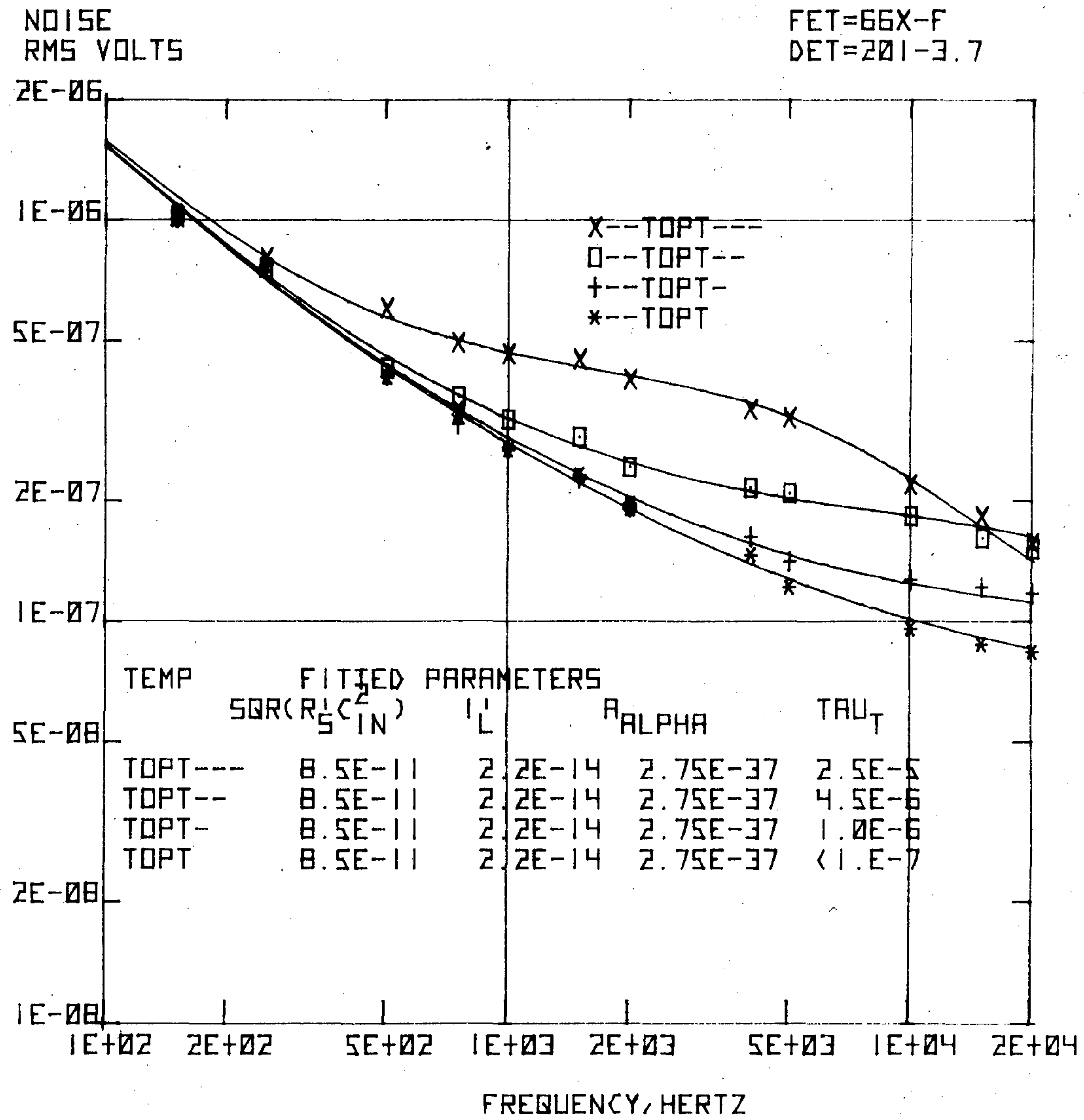

XBL 754-996

Fig. 15

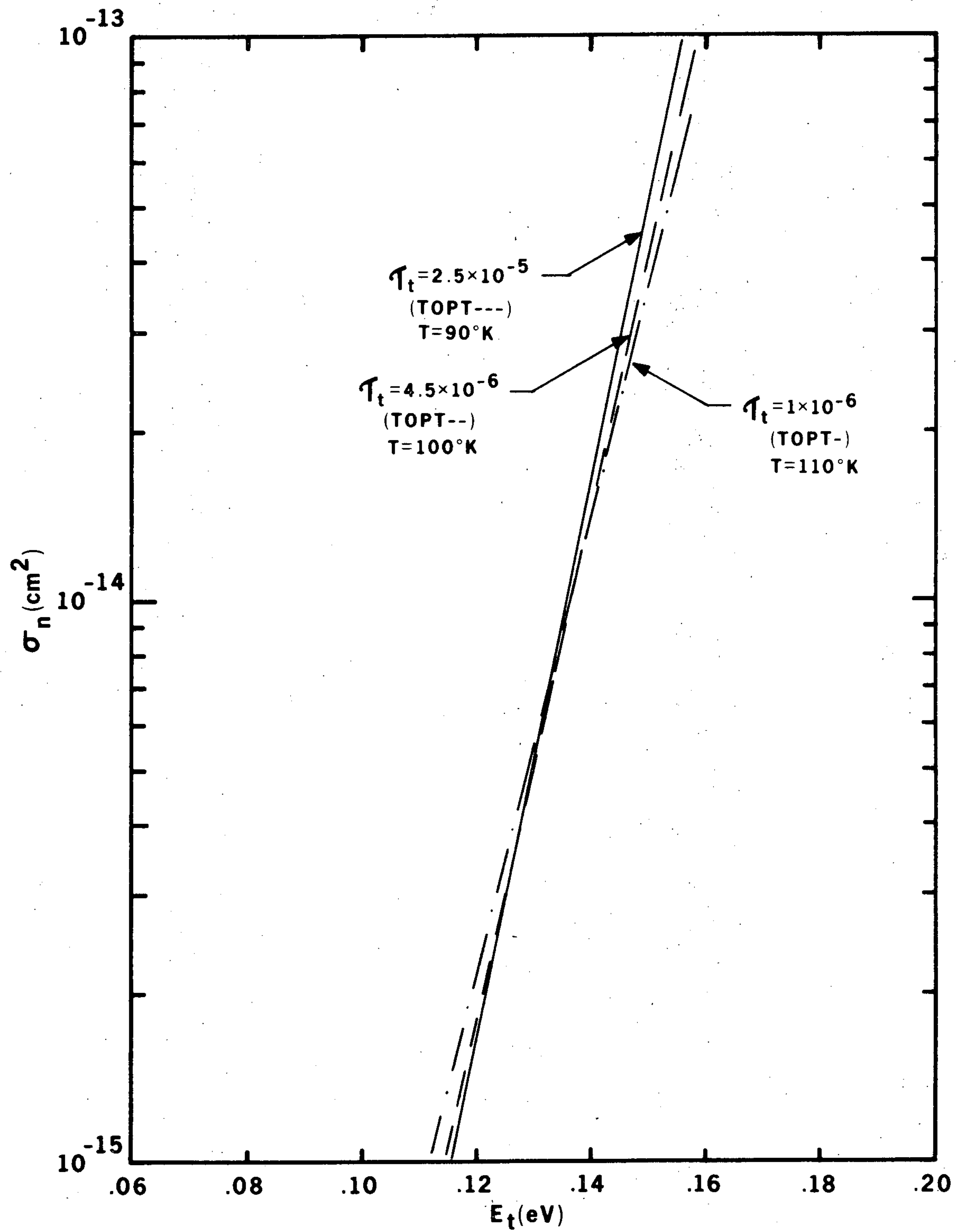

Fig. 16

0 0 0 4 3 0 1 4 7 2

LEGAL NOTICE

This report was prepared as an account of work sponsored by the United States Government. Neither the United States nor the United States Energy Research and Development Administration, nor any of their employees, nor any of their contractors, subcontractors, or their employees, makes any warranty, express or implied, or assumes any legal liability or responsibility for the accuracy, completeness or usefulness of any information, apparatus, product or process disclosed, or represents that its use would not infringe privately owned rights.

TECHNICAL INFORMATION DIVISION
LAWRENCE BERKELEY LABORATORY
UNIVERSITY OF CALIFORNIA
BERKELEY, CALIFORNIA 94720